Journal of Economic Dynamics & Control 113 (2020) 103855

Contents lists available at ScienceDirect

Journal of Economic Dynamics & Control

journal homepage: www.elsevier.com/locate/jedc

# Do 'complex' financial models really lead to complex dynamics? Agent-based models and multifractality

Jiri Kukacka[a,b,*], Ladislav Kristoufek[a,b]

[a] The Czech Academy of Sciences, Institute of Information Theory and Automation, Pod Vodarenskou vezi 4, 182 00 Prague 8, Czechia
[b] Faculty of Social Sciences, Institute of Economic Studies, Charles University, Opletalova 26, 110 00 Prague 1, Czechia

ARTICLE INFO

*Article history:*
Received 25 July 2019
Revised 15 December 2019
Accepted 26 January 2020
Available online 7 February 2020

*JEL classification:*
C13
C22
C63
D84
G02
G17

*Keywords:*
Complex systems
Financial agent-based models
Time series analysis
Multifractal analysis
Detrended fluctuation analysis

ABSTRACT

Agent-based models are usually claimed to generate complex dynamics; however, the link to such complexity has not been subject to rigorous examination. This paper studies this link between the complexity of financial time series—measured by their multifractal properties—and the design of various small-scale agent-based frameworks used to model the heterogeneity of financial markets. Nine popular models are analyzed, and while some of the models do not generate interesting multifractal patterns, we observe the strongest tendency towards multifractal behavior for the Bornholdt Ising model, the discrete choice-based models by Gaunersdorfer & Hommes and Schmitt & Westerhoff, and the transition probabilities-based framework by Franke & Westerhoff. Complexity is thus not an automatic feature of the time series generated by any agent-based model but generated only by models with specific properties. In addition, because multifractality is considered a financial stylized fact, its presence can be used as a new means to validate such models.



## 1. Introduction

Financial markets have proven to be very complicated systems of competing and interacting economic agents with heterogeneous motives, strategies and investment horizons. Such interplays create highly complex dynamics that are hard to model and predict with the linear models that play an essential role in financial economics and related fields (Chen et al., 2012; Hu et al., 2019; Shang, 2014). Nonlinear agent-based models, usually built on simple heuristic rules of agents' behavior, have become popular in various fields of the social sciences over the last two decades, as they provide a more realistic description of society and its functioning. In economics and particularly in finance, these models have been shown to successfully replicate the traditional stylized facts of financial markets (Cont et al., 2007). Not only are financial agent-based models able to mimic the statistical and dynamic properties of financial time series; they also allow for a more detailed discussion of the connection between their construction design and the system dynamics they produce, potentially including multifractal behavior of financial time series.

* Corresponding author at: The Czech Academy of Sciences, Institute of Information Theory and Automation, Pod Vodarenskou vezi 4, 182 00 Prague 8, Czechia.
*E-mail addresses:* kukacka@utia.cas.cz (J. Kukacka), kristoufek@utia.cas.cz (L. Kristoufek).

https://doi.org/10.1016/j.jedc.2020.103855
0165-1889/

Multifractality is a statistical characteristic of a sequence or time series connected to its complex scaling properties. Extending the fractality characteristic by describing scaling properties of the series with a single exponent, multifractality in a series explains complex behavior by a spectrum of exponents. This leads to possibly very complex dynamics of the series that are difficult to describe but interesting for a broad range of disciplines, including hydrometeorology (Veneziano et al., 2006), medicine (Lopes and Betrouni, 2009), image processing (Arneodo et al., 2000), geochemistry (Zuo and Wang, 2016), geology (Dellino and Liotino, 2002), climate change (Ashkenazy et al., 2003) and others. One of the very fruitful fields of study with respect to multifractality is finance. In addition to many empirically oriented studies (Barunik et al., 2012; Di Matteo, 2007; Di Matteo et al., 2003; 2005; Liu et al., 2007; Lux and Kaizoji, 2007; Zhou, 2009), there have been many statistically oriented ones focusing on possible sources of multifractality in financial time series including stock markets, foreign exchange rates, interest rates, commodities, and others, specifically their returns, volatility, volume, and liquidity.

In this vein, it has been shown that various statistical and dynamic characteristics can be identified as sources of 'real' or 'apparent' multifractality. Among these, there are fat tails (Chechkin and Gonchar, 2000; Nakao, 2000), distribution broadness (Zhou, 2009), finite sample size (Grech and Pamuła, 2012; 2013; Pamuła and Grech, 2014), and various correlation structures (Buonocore et al., 2016; Kantelhardt, 2009; Kantelhardt et al., 2002; Theiler et al., 1992). Much space has thus been given to exploring statistical and econometric sources of multifractality, and these sources can be seen as well understood, as documented in a recent review by Jiang et al. (2018). Multifractality has actually been labeled a new stylized fact of the financial markets (Lux and Segnon, 2018) in addition to the standard stylized facts listed by Cont (2001) such as the vanishing of the returns autocorrelation, volatility clustering, or non-Gaussian and fat-tailed distributions of the returns. However, little to no attention has been given to structural, qualitative sources of multifractality in financial time series.

As the multifractal framework has served as a basis for various models (Bacry et al., 2008; Calvet and Fisher, 2001; Lux, 2008; Mandelbrot et al., 1997), we suggest that the presence of multifractality can potentially be used as one of the new means of validation of financial agent-based models in general (Fagiolo et al., 2019; Lux et al., 2018; Platt, 2019; Windrum et al., 2007). This paper thus focuses on a connection between multifractality and complexity of financial time series and examines multifractality as its measure. As complexity is a very broad term in the context of time series modeling, we here specify it as a complicated nonlinear correlation structure originating from the heterogeneity of financial markets. Heterogeneity of markets is here synonymous with heterogeneity of market participants, specifically their trading strategies, investment horizons and sensitivity to local and/or global influences.

Nine popular elementary financial agent-based models are analyzed. The list of the 'model zoo' begins with one of the oldest small-scale models in the literature introducing the concept of behavioral heterogeneity among financial market participants, the cusp catastrophe model by Zeeman (1974); this model is followed by the seminal Brock and Hommes (1998) heterogeneous agent model that is further extended by Gaunersdorfer and Hommes (2007), which dynamics are governed by the multinomial logit discrete choice formula for the adaptive switching of economic agents between available trading strategies. The spin model by Bornholdt (2001) parallelizes a financial market to the ferromagnetic model, and the model by Gilli and Winker (2003) built in the 'ant dynamics' tradition of Kirman (1993) introduces the concept of transition probabilities. Models by Alfarano et al. (2005, 2008) provide extended concepts of modeling financial herding based on the asymmetric transitions probabilities and the Langevin equation approximation. Finally, we study the recent concept by Franke and Westerhoff (2011) that extends the famous 'interactive agent hypothesis' with a structural volatility component; one of the most recent approaches by Schmitt and Westerhoff (2017) is a computationally simplified version of a large-scale 'structural volatility' model with mutually dependent individual stochastic terms and the occurrence of sunspots that may trigger extreme events. By connecting these models with the multifractal framework, we verify the existence of multifractal behavior within artificial agent-based financial markets. Moreover, using predominantly the simulation-based approach, we elegantly bypass complications with parameter estimation (Grazzini and Richiardi, 2015; LeBaron and Tesfatsion, 2008; Recchioni et al., 2015).

The model contest paper by Franke and Westerhoff (2012) might, to some extent, be considered a conceptual precursor to our multifractal analysis. The authors, however, concentrate specifically on so-called 'structural stochastic volatility' models under the transition probabilities-based and the discrete choice-based approach. The main goal of the analysis then lies in their replication capability of the important stylized facts and empirical moments within the framework of the simulated method of moments.

An extensive Monte Carlo simulation study utilizes the toolkit of the multifractal detrended fluctuation analysis (MF-DFA), the multifractal detrended moving average method (MF-DMA), and the generalized Hurst exponent method (GHE) estimation. To distinguish whether a potential multifractality is due to agent-based linear and nonlinear correlation structure or distributional properties of the underlying process, we compare the result of the original series with the randomly shuffled series. While some models mostly appear to suffer from a small-size effect potentially influencing multifractal properties and do not generate other interesting multifractal patterns, we observe the strongest tendency towards multifractal behavior for the Bornholdt (2001) Ising model, the discrete choice-based models by Gaunersdorfer and Hommes (2007) and Schmitt and Westerhoff (2017), and the transition probabilities-based framework by Franke and Westerhoff (2011).

## 2. Multifractality and its estimation

### 2.1. Multifractality formalism

Multifractality is one of the concepts developed outside of economics and finance but widely expanding to other scientific disciplines. From a time-series analysis perspective, multifractality can be seen as a generalization of long-range dependence. Long-range dependent processes have an asymptotically hyperbolically (power-law) decaying autocorrelation function $\rho(k) \propto k^{2H-2}$ for a time lag $k \to +\infty$ with a decay given by the Hurst exponent $H$ (Beran, 1994). The value of $H = 0.5$ represents an asymptotically uncorrelated process, while $H > 0.5$ and $H < 0.5$ imply persistent and antipersistent processes, respectively. This property of the autocorrelation function leads to a power-law scaling of the variance of the integrated process with increasing time series length (Samorodnitsky, 2006). Long-range dependent processes, sometimes also labeled fractal processes, are thus characteristic of a specific scaling of the second moment. The multifractal framework generalizes this approach for the $q$th moments, where $q \in \mathbb{R}$, so that a spectrum of the generalized Hurst exponents $H(q)$ is necessary for a full description of dynamics and scaling behavior of multifractal time series (Kantelhardt, 2009).

According to Calvet and Fisher (2002), a stochastic process $\{X_t\}$ is called multifractal if it has stationary increments and it holds that:

$$\mathbb{E}(|X_t|^q) = c(q)t^{\tau(q)+1}. \tag{1}$$

Here, $\tau(q)$ is the scaling function of the multifractal process, which is linear for unifractal (monofractal) processes and concave for multifractal processes, and $q$ is the moment order. The scaling function $\tau(q)$ can be translated into the language of the generalized Hurst exponents $H(q)$ as:

$$H(q) = \frac{1+\tau(q)}{q}. \tag{2}$$

For $q = 2$, the generalized Hurst exponent becomes the Hurst exponent of long-range dependence, i.e., the scaling parameter of the power-law decay of the autocorrelation function of long-range dependent (persistent) processes (Buonocore et al., 2016; Di Matteo, 2007; Di Matteo et al., 2005). The concavity of the scaling function $\tau(q)$ of multifractal processes translates into decreasing $H(q)$ with $q$. The range of the generalized Hurst exponents is then used as a measure of multifractality of the underlying time series. Alternatively, singularity strength $\alpha$ and singularity spectrum $f(\alpha)$, defined as:

$$\alpha = \frac{\partial\tau(q)}{\partial q} \text{ and } f(\alpha) = q\alpha - \tau(q), \tag{3}$$

particularly the width of the spectrum, are used to measure the level of multifractality. The relationship between all three components can be then written as (Kantelhardt, 2009):

$$\alpha(q) = H(q) + qH'(q) \text{ and } f(\alpha) = q(\alpha - H(q)) + 1. \tag{4}$$

As a measure of the level of multifractality, that is, a measure of complexity of the system, we use the range of the generalized Hurst exponents $\Delta H \equiv \max_q H(q) - \min_q H(q)$ and the width of the multifractal spectrum $\Delta\alpha \equiv \max_q \alpha(q) - \min_q \alpha(q)$. The larger either of these measures is, the higher the level of multifractality of the underlying series is. In finance, multifractality is mostly examined with respect to the returns or volatility series (Jiang et al., 2018). Some studies also focus on logarithmic prices which is parallel to studying returns series as logarithmic prices are simply integrated logarithmic returns series.

### 2.2. Generalized Hurst exponent estimators

We utilize three estimators of the generalized Hurst exponent $H(q)$, specifically, the MF-DFA, MF-DMA, and GHE methods.[1] We opt for these three time-domain estimators as they provide a good balance between low number of parameters and efficiency (Kantelhardt, 2009).

MF-DFA is a multifractal generalization of the detrended fluctuation analysis (Kantelhardt et al., 2002; Peng et al., 1993) that is based on scaling of detrended variances of the integrated long-range dependent processes, specifically the power-law relationship between the detrended variance and the series length. This translates into the scaling law between average variance estimated on subsamples of a given length of the original series. The size of these subsamples is standardly referred to as scale $s$ (as the subsamples are of the length $s$). For the given scale $s$, we split the series into $N_s$ nonoverlapping boxes (as we can split from both ends of the series, we obtain $2N_s = 2\lfloor T/s \rfloor$, where $T$ is the time series length and $\lfloor . \rfloor$ is the nearest lower integer operator; if the time series length is divisible by the scale, we have $N_s = T/s$ non-overlapping boxes), and in each box $\nu$, we obtain a mean squared error from a trend (usually linear) $F^2_{DFA}(\nu, s)$, which is averaged over all boxes of scale $s$ as:

$$F_q(s) = \left(\frac{1}{2N_s}\sum_{\nu=1}^{2N_s}(F^2_{DFA}(\nu, s))^{q/2}\right)^{1/q}. \tag{5}$$

[1] Supplementary material associated with this article containing R codes for the estimators of the generalized Hurst exponent together with three illustrative examples of the estimation procedure can be found, in the online version, at doi: 10.1016/j.jedc.2020.103855.

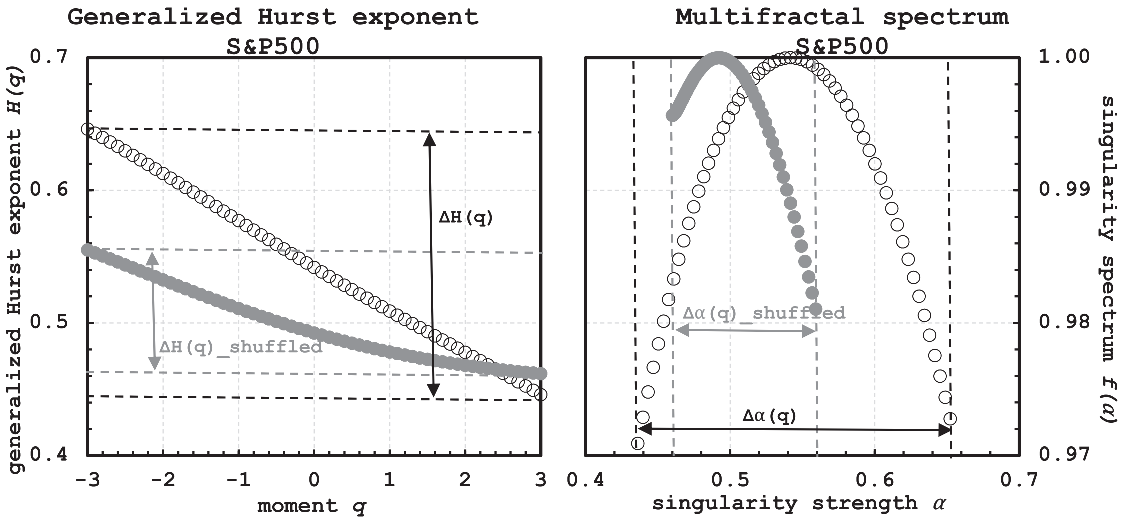


**Fig. 1.** Empirical example—S&P 500 index. *Note:* Multifractal properties of the S&P 500 stock index logarithmic returns between 1 Jan 2014 and 30 Sep 2019 (1,446 observations) are illustrated by the MF-DFA estimator, specifically the generalized Hurst exponent (left) and the multifractal spectrum (right). The estimator settings follow the descriptions in the text that are later used in the simulations.

The generalized Hurst exponent $H(q)$ is then obtained through the scaling law:

$$F_q(s) \propto s^{H(q)}. \tag{6}$$

The details of the MF-DFA procedure are given in Kantelhardt et al. (2002, pg. 89–91). MF-DMA is built on a similar idea as MF-DFA, but rather than using polynomial detrending, it is based on detrending and then scaling via the moving averages (Alessio et al., 2002; Kantelhardt, 2009). Again, MF-DMA is based on a unifractal detrending moving average method of Vandewalle and Ausloos (1998). The fluctuation functions and the scaling behavior are parallel to (5) and (6), only the $F^2_{DMA}(\nu, s)$ function represents a mean squared error from the moving average of length $s$ for the given box $\nu$ compared to the deviations from the time trend in the case of $F^2_{DFA}(\nu, s)$. The basics are laid by Alessio et al. (2002, pg. 198) and further generalized by Jiang and Zhou (2011, pg. 2).

The GHE procedure is different from the other two as it mostly builds on fractal geometry. In the time series (and here specifically financial) context, it was introduced in the series of papers by Di Matteo et al. (2003, 2005) and Di Matteo (2007). Multifractal features are obtained from scaling of the $q$-order moments of the distribution of the increments of the integrated process $X$. Specifically, we have the scaling function:

$$K_q(\tau) = \frac{\langle |X(t+\tau) - X(t)|^q \rangle}{\langle |X(t)|^q \rangle} \tag{7}$$

and the generalized Hurst exponent is obtained from the scaling law:

$$K_q(\tau) \propto \tau^{qH(q)}. \tag{8}$$

For each of these estimation procedures, the scaling range on which the generalized Hurst exponent is estimated needs to be specified. We follow industry standards and use $s_{min} = 10$ and $s_{max} = T/10$, where $T$ is the length of a time series, for MF-DFA with a step between scales of 10. For MF-DMA, we select comparable setting with $s_{min} = 11$ and $s_{max} = (T/10) + 1$ as we use the centered moving averages for filtering. In addition, for GHE, we use $\tau_{min} = 1$, and we vary $\tau_{max}$ between 5 and 20 (or 100 for longer time series); the final estimator is based on the average of the estimators using this range, i.e., practically using the jackknife method as suggested by Di Matteo et al. (2003, p. 184–186).

### *2.3. Two empirical examples*

As simple illustrations, we briefly study the multifractal properties of two selected financial time series. We examine the daily logarithmic returns of the S&P 500 stock index and Bitcoin as the dominant cryptocurrency. Each is studied between January 1, 2014, and September 30, 2019, with 1446 and 2099 observations, respectively (Bitcoin is traded 24 h a day, 7 days a week).[2] In Figs. 1 and 2, we present the range of the generalized Hurst exponents and the multifractal spectra of the studied assets. These are shown only for MF-DFA to save space. We see that the multifractal measures shrink for the shuffled

[2] Supplementary material associated with this article containing R code and empirical data used in Section 2.3 can be found, in the online version, at doi: 10.1016/j.jedc.2020.103855.

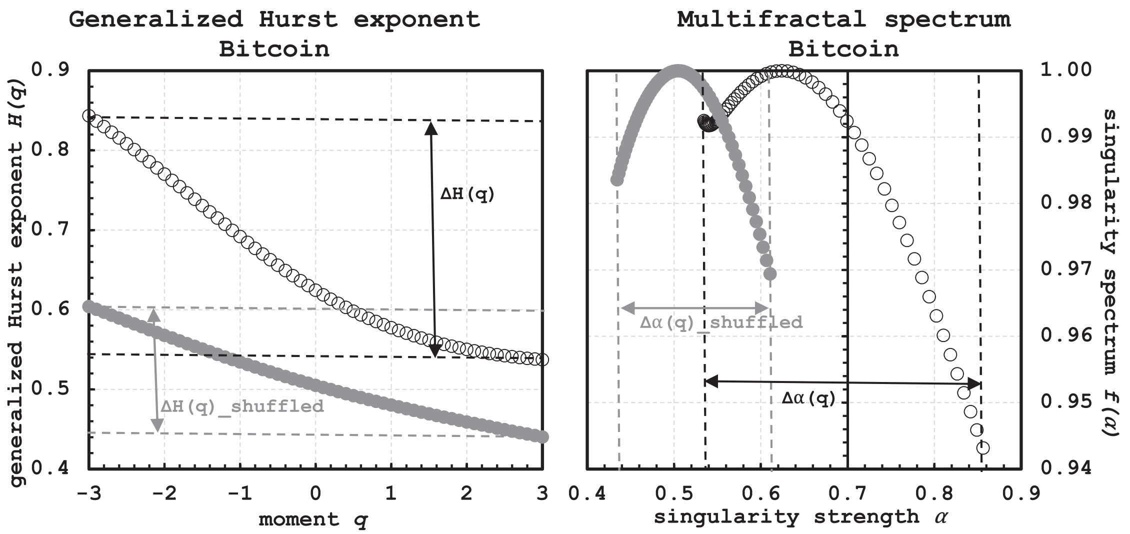


**Fig. 2.** Empirical example—Bitcoin. *Note:* Multifractal properties of Bitcoin logarithmic returns (CoinMarketCap.com [accessed 2019-11-08] volume-average price) between 1 Jan 2014 and 30 Sep 2019 (2,099 observations) are illustrated by the MF-DFA estimator, specifically the generalized Hurst exponent (left) and the multifractal spectrum (right). The estimator settings follow the descriptions in the text that are later used in the simulations.

**Table 1**
Multifractal measures for S&P 500 and Bitcoin—generalized Hurst exponent.

| Estimator | $\Delta H$ | $\Delta H_{shuffled}$ | $q_{0.05}$ | $q_{0.95}$ |
|---|---|---|---|---|
| S&P 500 | | | | |
| MF-DFA | 0.2083 | 0.1009 | 0.0391 | 0.1544 |
| MF-DMA | 0.2266 | 0.1248 | 0.0280 | 0.2467 |
| GHE | 0.0566 | 0.1569 | 0.1165 | 0.1968 |
| BTC | | | | |
| MF-DFA | 0.3063 | 0.1235 | 0.0615 | 0.1794 |
| MF-DMA | 0.2746 | 0.1094 | 0.0286 | 0.2171 |
| GHE | 0.1496 | 0.2153 | 0.1797 | 0.2496 |

**Table 2**
Multifractal measures for S&P 500 and Bitcoin—multifractal spectrum.

| Estimator | $\Delta\alpha$ | $\Delta\alpha_{shuffled}$ | $q_{0.05}$ | $q_{0.95}$ |
|---|---|---|---|---|
| S&P 500 | | | | |
| MF-DFA | 0.2242 | 0.1089 | 0.0431 | 0.1670 |
| MF-DMA | 0.2467 | 0.1345 | 0.0320 | 0.2635 |
| GHE | 0.0545 | 0.1542 | 0.1141 | 0.1926 |
| BTC | | | | |
| MF-DFA | 0.3217 | 0.1330 | 0.0669 | 0.1944 |
| MF-DMA | 0.2908 | 0.1180 | 0.0324 | 0.2338 |
| GHE | 0.1486 | 0.2100 | 0.1744 | 0.2439 |

series when the correlation structure is torn. Nevertheless, some level of multifractality remains due to the distributional properties that remain unchanged after shuffling. The multifractal properties of Bitcoin seem more pronounced because the measures for original series point not only to higher complexity in Bitcoin compared to the S&P index but also to the wider distribution as both the multifractal spectrum and the generalized Hurst exponents range are wider for the cryptocurrency. These results are not too surprising when comparing a stock index and a cryptocurrency.

The figures represent the results for a single shuffled series to distinguish between the distributional and complexity causes of multifractality. Even though a single resampling is usually used for graphical purposes, statistical validity is ensured only through a repeated resampling and comparison of the multifractal properties of the original series with a large number of results for the shuffled series. In Tables 1 and 2, we summarize the results for all three estimators for the original series and for 1000 shuffled samples to identify the sources of multifractality with statistical validity. There are several interesting observations from the results. First, the GHE estimator delivers confusing results because the multifractal level of the original series is markedly (and significantly) lower than the one of the shuffled series. We discuss this issue further during the presentation of the simulation results, which show the same pattern. Second, the multifractality level of Bitcoin is higher than the one of the stock index for all estimators and both measures. Third, the major source of multifractality is not completely clear because the estimates for the stock index based on MF-DMA touch the 95% critical value (the 95th quantile of the shuffled series results). This result might be connected to the rather short sample we study here, which was, however, chosen due to the limited time series length for Bitcoin. In the simulations, we also focus on the effect of the time series length on the estimates. Fourth, the estimators, at least for these time series lengths, have considerable variance, as the wide quantiles suggest, which shows only how important it is to compare the multifractal estimates with a high number of shuffled repetitions. Nevertheless, both series show signs of multifractality above the trivial one due to the distribution broadness.

## 3. Model zoo

We briefly present the 'model zoo' consisting of nine famous and widely analyzed elementary financial agent-based models. Our choice is driven by an effort to encompass various types of modeling approaches and mechanisms triggering endogenous evolutionary dynamics. The list begins with one of the oldest small-scale models in the literature introducing the concept of behavioral heterogeneity among financial market participants, the cusp catastrophe model by Zeeman (1974), and ends with one of the most recent approaches by Schmitt and Westerhoff (2017) that is a computationally simplified version of a large-scale model in which the individual stochastic terms are not independent and the model dynamics are influenced by the occurrence of sunspots that may trigger extreme events.

### 3.1. Cusp catastrophe model

Catastrophe theory by Thom (1975) suggests a stylized but appealing general principle of how gradual continuous changes in control variables of a system may lead to a rapid discontinuous change from one system equilibrium to another. We focus on one of the simplest specifications, the cusp catastrophe model proposed by Zeeman (1974), to model abrupt stock market crashes. This application of the cusp model can be rightfully considered one of the first financial agent-based models in the literature as the model directly builds on a dynamic interaction between fundamentalists and chartists in the stock market.

The cusp model extended by Cobb (1981) simulates a stochastic time-variant process $y_t$ as $\mathrm{d}y_t = -\frac{\mathrm{d}(1/4y_t^4+1/2\beta_{z,t}y_t^2+\alpha_{z,t}y_t)}{\mathrm{d}y_t}\mathrm{d}t + \sigma_{y_t}\mathrm{d}W_t$, where $\alpha_{z,t}$ and $\beta_{z,t}$ are the control variables, formulating the deterministic term of the process that represents the equilibrium state of the model; $\sigma_{y_t}$ is the diffusion function, and $W_t$ is the Wiener process, together formulating the stochastic term. In addition, the $\alpha_{z,t}$ and $\beta_{z,t}$ dimensions of the control space linearly depend on realizations of $n$ independent variables $z_{i,t}$, $i = 1\ldots,n$, $t = 1\ldots,T$, as: $\alpha_{z,t} = \alpha_0 + \sum_{i=1}^{n}\alpha_i z_{i,t}$ and $\beta_{z,t} = \beta_0 + \sum_{i=1}^{n}\beta_i z_{i,t}$.

The linear control functions $\alpha_{z,t}$ and $\beta_{z,t}$ are called asymmetry and bifurcation factors, and in a stock market application, they represent the fundamental and the speculative side of the market, respectively. By virtue of the mathematical form of the model, there can be up to three equilibria of the potential function determining the predicted value of $y_t$ given by roots of $-y_t^3 + \beta_{z,t}y_t + \alpha_{z,t} = 0$. In the case of three roots, the central one is the least probable state of the system, and the state variable $y_t$ is thus bimodal.

As the stochastic catastrophe theory restrictively assumes a constant diffusion function, $\sigma_{y_t} = \sigma$, Kukacka and Barunik (2013) propose a rigorous solution allowing for its general application in modeling stock market crashes, although the diffusion function in such a case represents a highly dynamic volatility of stock market returns with a strong clustering property, $\sigma_{y_t} = \sigma_t$. It is suggested that daily stock returns normalized by their consistently estimated volatility follow a stochastic cusp catastrophe process $\mathrm{d}y^* = -\frac{\mathrm{d}(1/4y_t^{*4}+1/2\beta_{z,t}y_t^{*2}+\alpha_{z,t}y_t^*)}{\mathrm{d}y_t^*}\mathrm{d}t + \mathrm{d}W_t$, where the diffusion function $\sigma_{y_t} = 1$ and the maximum likelihood estimator of the model parameters suggested by Cobb (1981) can be conveniently used. The normalization of the stock returns can be done, e.g., using the concept of realized volatility (Barunik and Kukacka, 2015), or even more simply via GARCH modeling. The suggested approach simulates the data from the stochastic cusp catastrophe model under the assumption of time-varying volatility:

$$\mathrm{d}y_t = (\alpha_{z,t} + \beta_{z,t}y_t - y_t^3)\mathrm{d}t + \mathrm{d}W_{1,t}, \tag{9}$$

$$\mathrm{d}\sigma_t^2 = \kappa(\omega - \sigma_t^2)\mathrm{d}t + \zeta\mathrm{d}W_{2,t}, \tag{10}$$

$$r_t = \sigma_t y_t, \tag{11}$$

where (9) represents the equilibrium surface of the cusp potential function and $dW_{1,t}$, $dW_{2,t}$ are the uncorrelated standard Brownian motions. (10) further independently simulates a time-varing volatility process with the initial $\sigma_1^2 = 0.3$, and following Zhang et al. (2005), we set $\kappa = 5,\ \omega = 0.04,\ \zeta = 0.5$ as reasonable values for a stock. The parameters of the volatility process in (10) thus satisfy the Feller's condition $2\kappa\omega \geq \zeta^2$, keeping the volatility away from the zero lower bound. Finally, (11) interconnects these two concepts so that $r_t$ stands for discrete-time volatility-adjusted log-returns generated by cusp. We further use $n = 2$ independent variables drawn from the uniform $U(0,\ 1)$ distribution with coefficients $\alpha_j = \{-2, 3, 0\}$ and $\beta_j = \{-1, 0, 4\}$, $j = \{0, 1, 2\}$. The nought values of $\alpha_2$ and $\beta_1 = 0$ ensure that $z_{1,t}$ drives only the asymmetry side of the model, and $z_{2,t}$ solely determines the bifurcation side.

### 3.2. Brock and Hommes (1998) heterogeneous agent model (BH)

The famous Brock and Hommes (1998) model represents the most frequently applied financial agent-based model framework. The model suggests a financial market application of a stylized endogenous evolutionary selection among a set of heterogeneous trading strategies. In principle, it is a heterogeneous expectations (Lucas, 1978) feedback system, the dynamics of which depend on both the known values of the model variables and the future expectations of the market participants. The analyzed system consists of four interdependent equations, the derivation of which can be found in Hommes et al. (2006):

$$Ry_t = \sum_{h=1}^{H} x_{h,t-1} f_{h,t} + \varepsilon_t \equiv \sum_{h=1}^{H} x_{h,t-1}(g_h y_{t-1} + b_h) + \varepsilon_t, \tag{12}$$

$$x_{h,t-1} = \frac{\exp(\gamma U_{M,h,t-1})}{\sum_{h=1}^{H} \exp(\gamma U_{M,h,t-1})}, \tag{13}$$

$$U_{h,t-1} = (y_{t-1} - Ry_{t-2}) \frac{f_{h,t-2} - Ry_{t-2}}{a\sigma^2}, \tag{14}$$

$$U_{M,h,t-1} = U_{h,t-1} + \delta U_{M,h,t-2} - C_h. \tag{15}$$

(12) is a pricing formula for a risky asset determining a heterogeneous market equilibrium price level $p_t$, $t = 1, \ldots, T$, in the form of deviations from the constant fundamental price $\bar{p}$, $y_t = p_t - \bar{p}$. $R = 1 + r$ represents the constant risk-free gross interest rate. Market fractions of agents of type $h \in \{1, \ldots, H\}$ at time $t-1$ are denoted as $x_{h,t-1}$, satisfying $\sum_{h=1}^{H} x_{h,t-1} = 1$. A deterministic function $f_{h,t} = g_h y_{t-1} + b_h$ defines a '$h$-type' trading strategy at time $t$, where $g_h$ and $b_h$ are the trend and bias parameters. Fundamental traders are represented by $g_h = b_h = f_{h,t} = 0$, i.e., they expect the risky asset price to always converge to its fundamental values $\bar{p}$. Conversely, chartists utilize extrapolation techniques and simple technical trading rules via various combinations of $g_h \gtreqless 0$ and $b_h \gtreqless 0$. The error term $\varepsilon_t$ is an independent and identically distributed (i.i.d.) sequence that accounts for the stochastic nature of the market. (13) determines the fraction of agents following trading strategy $h$, $x_{h,t-1}$, under the discrete choice probability framework. $U_{M,h,t-1}$ is the past profitability of strategy $h$, and $\gamma \geq 0$ is the intensity of choice governing the willingness of agents to switch between alternative trading strategies. The past profitability, $U_{M,h,t-1}$, is derived in (14) and (15) as a weighted average of the past realized values, risk-aversion coefficient $a > 0$, and conditional variance $\sigma^2$. Here, $0 \leq \delta \leq 1$ represents the 'information dilution principle' or simply a 'Memory' of traders, and $C_h \geq 0$ is the cost of obtaining market information.

The computational design follows Kukacka and Barunik (2013), Kukacka and Barunik (2017), Polach and Kukacka (2019): $R = 1 + r = 1.0001$, the linear scale factor $1/a\sigma^2 = 1$, $H = 2$, $g_1 = b_1 = 0$, $g_2 = 0.4$, $b_2 = 0.3$. This means we analyze the most simple version of the model with only two types of traders and fixed belief coefficients. The intensity of choice $\gamma = 10$, the noise term is randomly drawn from the standard normal distribution, and the dilution parameter $\delta = 0.99$ as suggested in Gaunersdorfer and Hommes (2007). Following Hommes et al. (2006), $C_h = 0$ for $h = \{1, 2\}$.

### 3.3. Bornholdt (2001) Ising model

The spin model by Bornholdt (2001) is an adjusted version of the basic Ising model suggested for modeling a financial market that is parallelized to the ferromagnetic model through the market participants representing spins with a positive (buyers, $+1$) or a negative (sellers, $-1$) value organized in a squared lattice $L \times L$. The spin value dynamically updates according to the heat-bath dynamics so that a market participant $S_{j,t+1}$ is a buyer with a probability $P_{i,t} = 1/\big(1 + \exp(-2\beta h_{i,t})\big)$, where $\beta$ is a responsiveness parameter, and a seller with a probability $1 - P_{i,t}$. The interplay between the global and the neighboring influence is defined as the value of the local field $h_{i,t}$ specified as:

$$h_{i,t} = \sum_{j=1}^{L^2} J_{i,j} S_{j,t} - \alpha C_{i,t} \left| \frac{1}{L^2} \sum_{j=1}^{L^2} S_{j,t} \right|, \tag{16}$$

where $S_{j,t}$ is the value of the $j$th spin, $j = 1 \ldots, L^2$, at time $t = 1 \ldots, T$, and $J_{i,j} = 1$ for close neighbors and zero otherwise. $\alpha > 0$ is a global coupling parameter, and $C_{i,t}$ is a strategy of spin $i$ at time $t$. Parameters are set according to Kristoufek and Vosvrda (2018): $\alpha = 4,\ \beta = 2/3,\ L = 32$. The first part of the equation represents a local Ising Hamiltonian, usually specified by the nearest neighbors, and the second part describes the reaction to the global price, which resembles the minority game. The connection to financial markets follows the formula for financial log-returns:

$$r_t = \log p_t - \log p_{t-1} = \frac{1}{L^2} \sum_{j=1}^{L^2} S_{j,t} - \frac{1}{L^2} \sum_{j=1}^{L^2} S_{j,t-1}. \tag{17}$$

A closely related model by Cont and Bouchaud (2000) also motivated by the original Ising framework explains a connection between the heavy tails observed in empirical distributions of financial returns and herding behavior of financial market participants. The work by da Silva and Stauffer (2001) then further analyzes the Ising-like stock market model by Cont and Bouchaud (2000) via simulations. Stauffer (2008) reviews three famous socio-economic models including the seminal Schelling (1971) model of segregation and, via numerical simulations, shows that the standard two-dimensional Ising model can provide similar results.

### 3.4. Gilli and Winker (2003) model of herding (GW)

The concept of herding behavior represents the second most frequently accepted principle of possible evolution of market fractions in financial agent-based models that can trigger interesting nonlinear endogenous dynamics resulting in large aggregate price fluctuations. The herding principle is based on direct interactions of agents in which members of one subpopulation can 'recruit' the other agents to join. Agents can also switch between the subpopulations randomly.

The model is designed in the 'ant dynamics' tradition introduced by Kirman (1991, 1993). Following the harmonized notation by Barde (2016), the model population consists of $N$ agents of the two coexisting subpopulations: fundamentalists ($f$) and chartists ($c$). Let $n_t$ represent the number of fundamentalists at time $t = 1, \ldots, T$. The fundamentalist population fractions are denoted as $x_t = n_t/N$. During each of $\tau$ interactions per trading day, three agents labeled $a_1$, $a_2$, and $a_3$ are randomly selected. Agent $a_1$ can be successfully recruited by $a_2$ to switch to her subpopulation with recruitment probability $\rho$ (if $a_1$ and $a_2$ are from the same subpopulation, nothing happens). Agent $a_3$ switches to the other subpopulation spontaneously with probability $\varepsilon$. Resulting transition probabilities govern the dynamic evolution of the system:

$$\begin{cases} P_t^{c\to f} = (1-x_t)(\varepsilon + \rho x_t), \\ P_t^{f\to c} = x_t(\varepsilon + \rho(1-x_t)). \end{cases} \tag{18}$$

However, agents in the Gilli and Winker (2003) model only have noisy private information about the fundamentalist population fraction, $\tilde{x}_t$, containing a measurement error, which is normally distributed $\tilde{x}_t \sim N(x_t, \sigma_x^2)$. The perceived fundamentalist population share is thus $\omega_t = P(\tilde{x}_t > 0.5)$. Expectations of the two subpopulations, from which the excess demand functions can be derived, are set as follows:

$$\begin{cases} E^f(\Delta p_t) = d_t^f = \phi(\bar{p} - p_{t-1}), \\ E^c(\Delta p_t) = d_t^c = p_{t-1} - p_{t-2}, \end{cases} \tag{19}$$

where $\phi$ in the fundamentalists' expectations is the adjustment speed to the fundamental value $\bar{p}$, while chartists simply extrapolate the past price change. The dynamic evolution of the market price finally follows:

$$p_t = p_{t-1} + \omega_t \phi(\bar{p} - p_{t-1}) + (1-\omega_t)(p_{t-1} - p_{t-2}) + u_t, \tag{20}$$

where $u_t \sim N(0, \sigma_s^2)$ is an i.i.d. price shock. As (20) describes the price evolution at the time-scale level of agents' interaction, one needs to pick only the $\tau$th observation from the generated time series to produce a daily series comparable to empirical observations.

The computational design follows the original (Gilli and Winker, 2003) setups summarized in Barde (2016): the population consists of $N = 100$ agents, $\tau = 50$ interactions per trading day, switching probabilities are set to $\rho = 0.264$ and $\varepsilon = 0.0001$, adjustment speed of fundamentalists $\phi = 0.0225$, and the fundamental value $\bar{p} = 1,000$. The standard deviation of the private information noise $\sigma_x = 0.219$, and the standard deviation of price shocks $\sigma_s = 0.25$.

### 3.5. Alfarano, Lux, and Wagner (2005) model of asymmetric herding (ALW05)

The Alfarano et al. (2005) model also follows the Kirman (1993) 'ant mechanics' framework that is generalized by asymmetric herding tendencies towards trading strategies. The model standardly assumes two distinct groups of $N$ market participants, $n_t$ fundamentalists ($f$) and $N - n_t$ noise traders/chartists ($c$), but compared to Gilli and Winker (2003), who update the fundamentalist population fraction $x_t$ based on directly simulating the interactions of agents, Alfarano et al. (2005) derive $x_t$ directly from the asymmetric transition probabilities:

$$\begin{cases} P_t^{c\to f} = (N - n_t)(\varepsilon_1 + n_t)\rho, \\ P_t^{f\to c} = n_t(\varepsilon_2 + (N - n_t))\rho, \end{cases} \tag{21}$$

where $\rho$ is a probability of a successful recruitment, and $\varepsilon_1$ and $\varepsilon_2$ are asymmetric probabilities of a spontaneous switch. The authors provide an analytical solution for $x_t$ in continuous time and obtain the master equation for large $N$ consisting of the drift and diffusion term:

$$x_{t+\Delta t} = x_t + \rho(\varepsilon_1 + \varepsilon_2)(\bar{x} - x_t)\Delta t + \lambda_t \sqrt{2\rho(1-x_t)x_t \Delta t}, \tag{22}$$

where $\bar{x} = \varepsilon_1/(\varepsilon_1 + \varepsilon_2)$ is the fundamentalists' mean population share and i.i.d. $\lambda_t \sim N(0, 1)$.

Fundamentalists believe in price reversion to its fundamental value $\bar{p}$, while chartists, compared to the Gilli and Winker (2003) model, are noise-traders. Their demand is governed by a random variable $\eta$, which follows either a bimodal distribution with values $\pm 1$ (spin noise model) or a uniform distribution over $U(-1, 1)$ (uniform noise model). Respective excess demand functions are given by:

$$\begin{cases} d_t^f = n_t(\bar{p} - p_t), \\ d_t^c = (N - n_t) r_0 \eta_t, \end{cases} \tag{23}$$

where $r_0$ is a scaling parameter for the price impact. Clearing the market to a zero sum of excess demand gives the formula for market log-returns:

$$r_t = r_0 \frac{x_t}{1 - x_t} \eta_t. \tag{24}$$

Parameters are set according to Alfarano et al. (2005) and summarized in Barde (2016) as follows: probabilities of a spontaneous switch $\varepsilon_1 = 16$, $\varepsilon_2 = 4.9$, herding tendency $\rho = 0.0025$, noise $\eta \sim U(-1, 1)$, and $r_0 = 0.015 \frac{\varepsilon_2 - 1}{\varepsilon_1}$.

### *3.6. Gaunersdorfer and Hommes (2007) model for volatility clustering (GH)*

The model by Gaunersdorfer and Hommes (2007) slightly modifies the original framework by Brock and Hommes (1998), while this adaptation provides a considerable improvement in terms of matching some stylized facts in financial time series data, especially volatility clustering. Building on the preceding description of the Brock and Hommes (1998) framework in Section 3.2, agents' expectations no longer follow the unified functional form $f_{h,t} = g_h(p_{t-1} - \bar{p}) + b_h$ that defines available trading strategies but, in a simple case with two types of traders ($H = 2$), the expected prices for fundamentalists [1] and trend-followers [2], respectively, are inspired e.g., by Frankel and Froot (1986) and given by:

$$\begin{cases} E_{1,t-1}[p_t] = f_{1,t} = \bar{p} + v(p_{t-2} - \bar{p}), \\ E_{2,t-1}[p_t] = f_{2,t} = p_{t-2} + w(p_{t-2} - p_{t-3}), \end{cases} \tag{25}$$

where $0 \le v \le 1$, $w \ge 0$, and $\bar{p}$ denote the fundamental price similarly to Section 3.2. A special case of fundamentalists are so-called Efficient Market Hypothesis believers who use a naive forecasting rule with $v = 1$, which is consistent with the efficient market hypothesis and prices following a random walk.

Moreover, the evolutionary updating of population fractions has two steps. The first follows (13), but the second considers a correction for the fraction of trend followers according the principle that as "*the fraction of technical traders decreases more, the further prices deviate from their fundamental value*" $\bar{p}$ (pg. 274):

$$\begin{cases} \tilde{x}_{2,t-1} = x_{2,t-1} \exp[-(p_{t-2} - \bar{p})^2/\psi], \\ \tilde{x}_{1,t-1} = 1 - \tilde{x}_{2,t-1}, \end{cases} \tag{26}$$

where $\psi > 0$. Hence, when prices deviate considerably from the fundamental value, the exponential correction decreases, which reflects growing concerns for trend followers about an impending price correction. On the other hand, when prices are close to the fundamental, population fractions of agents almost exactly follow the original discrete choice formula (13) based on the past profitability $U_{M,h,t-1}$ and the intensity of choice $\gamma$.

Parameters are set according to Gaunersdorfer and Hommes (2007) and Gaunersdorfer et al. (2008) as follows: $R = 1 + r = 1.001$, the linear scale factor $1/a\sigma^2 = 1$, $H = 2$, $v = 1$ $w = 1.9$, the fundamental price $\bar{p} = 1,000$, and the first four price deviations $y$ are initialized as equal to $-400$. The intensity of choice $\gamma = 2$, the noise term is randomly drawn from the normal distribution $N(0, 10^2)$, the dilution parameter $\delta = 0.99$, and $C_h = 0$ for $h = \{1, 2\}$.

Many other modifications of the original Brock and Hommes (1998) framework have been proposed. To name a few, Gaunersdorfer et al. (2008) adapt the Gaunersdorfer and Hommes (2007) model by utilizing accumulated risk-adjusted realized profits instead of net realized profits to calculate the past profitability performance measure but conclude that the dynamics of the adapted model are very similar. Franke (2010) suggests extending the Gaunersdorfer and Hommes (2007) model with an alternative noise process because the original additive specification of the noise in a price equation might result in artificial long memory patterns. The noise levels in the new 'structural stochastic volatility' approach are group-specific and proportional to the time-varying population fractions of fundamentalists and trend followers, which leads to the time-varying volatility of aggregate shocks to prices. The author concludes that in terms of the replication of selected stylized facts, noticeable improvement has been achieved, and in the long memory properties, in particular, the 'structural stochastic volatility' approach outperforms the more elaborate versions of the Brock and Hommes (1998) model proposed by Amilon (2008). Most recently, Schmitt (2019) considerably generalizes the Brock and Hommes (1998) framework by allowing all traders to follow their own time-varying trading strategies.

It can be seen via several examples in the previous paragraph that the field has made significant progress since the seminal contribution by Brock and Hommes (1998). Extended models have incorporated various sophisticated features, and their ability to replicate important stylized facts in financial time series data has generally increased over time. Since the Gaunersdorfer and Hommes (2007) model generates very interesting multifractal behavior, as seen in the following Section 4.2, we do not complicate our analysis with these more recent approaches that share the same background. However, we argue that they might exhibit even stronger or more interesting multifractal patterns.

### 3.7. Alfarano, Lux, and Wagner (2008) model (ALW08)

The Alfarano et al. (2008) model builds on the Alfarano et al. (2005) framework; however, it no longer assumes asymmetric herding, and the derivation as well as the notation of the model is altered. The population of fundamentalists consists of $n_f$ traders with an average trading volume $v_f$, and their excess demand is thus expressed as $d^f = n_f v_f(\bar{p}_t - p_t)$, where $\bar{p}_t$ is the log fundamental value and $p_t$ is the log-price at time $t$. The population of $n_c$ noise traders is characterized by a process of opinion changes, where an optimistic mood of a given agent at time $t$ is associated with buying $v_c$ units of the asset, and vice versa for a pessimistic mood. The population sentiment index is defined as $x_t = \frac{2n_{o,t}}{n_c} - 1$, where $n_{o,t}$ denotes the number of optimistic noise traders at time $t$, i.e., $x_t \in \langle -1, 1\rangle$. It is equal to zero for balanced sentiment and gains positive or negative values when the majority of noise traders are optimistic or pessimistic at time $t$, respectively.

The herding dynamics of the model are governed by a process of opinion changes within the population of noise traders, who dynamically switch between the optimistic and pessimistic regimes. The transition probabilities are given by the Poisson intensity $a \geq 0$ inducing autonomous switches of opinion and the rate $b \geq 0$ implying 'herding-based' switches caused by pairwise communication among noise traders. The sentiment dynamics process is characterized by a mean-reverting drift. Parameter $b$ being relatively high compared to $a$ results in strong majorities of optimistic or pessimistic noise traders over time, i.e., the system is characterized by a bimodal distribution of the sentiment index $x_t$. In such a case, the pairwise communication among noise traders leads the sentiment dynamics and is responsible for a persistent majority opinion. Conversely, if $a > b$, the sentiment index $x_t$ is dominantly governed by autonomous opinion changes, and therefore embodies a balanced situation, i.e., a unimodal unconditional distribution with its peak at 0. The complete continuous-time version model is summarized by four mutually dependent equations:

$$d\bar{p}_t = \sigma_f dB_{1,t}, \tag{27}$$

$$dx_t = -2ax_t dt + \sqrt{2b(1-x_t^2) + \frac{4a}{n_c}} dB_{2,t}, \tag{28}$$

$$p_t = \bar{p}_t + \frac{n_c v_c}{n_f v_f} x_t, \tag{29}$$

$$r_t = p_t - p_{t-1} \equiv \sigma_f e_t + \frac{n_c v_c}{n_f v_f}(x_t - x_{t-1}), \tag{30}$$

where $\bar{p}_t$ follows a standard Brownian motion without drift, $\sigma_f \geq 0$ denotes the standard deviation of innovations of $\bar{p}_t$; $B_{1,t}$ and $B_{2,t}$ stand for independent Wiener processes; $p_t$ and $r_t$ are the equilibrium market log-price and log-return at time $t$, respectively; and $e_t \sim$ i.i.d. standard normal distribution $N(0, 1)$ as the fundamental value for a unit time change associated with daily data, i.e., $\bar{p}_{t+1}$, can be obtained by a normal distribution $N(\bar{p}_t, \sigma_f)$.

The computational design follows Ghonghadze and Lux (2016), Chen and Lux (2018) and the Langevin equation aggregate approximation of the model in which $n_c = 100$, $\frac{n_c v_c}{n_f v_f} = 1$, $\sigma_f = 0.03$, $a = 0.0003$ and $b = 0.0014$ for the bimodal case utilized in this paper, and vice versa for the unimodal case.

### 3.8. Franke and Westerhoff (2011) structural stochastic volatility model (FW)

The model by Franke and Westerhoff (2011, 2016) also follows the herding mechanism tradition of Kirman (1993) amended by a noise term in each of the demand components of the two distinct groups of market agents. The model standardly assumes $N$ market participants, $n_t$ fundamentalists ($f$) and $N - n_t$ chartists ($c$) but defines the majority index of the fundamentalists as $x'_t = (2n_t - N)/N$, which is by construction contained between $-1$ and 1 for a market completely occupied by chartists and fundamentalists, respectively. Transition probabilities are defined as:

$$\begin{cases} P_t^{c\to f} = \nu exp(s_t), \\ P_t^{f\to c} = \nu exp(-s_t), \end{cases} \tag{31}$$

where $\nu$ is a flexibility parameter and $s_t$ is the switching index indicating the propensity to switch, defined as $s_t = a_0 + a_{x'} x'_{t-1} + a_d(p_{t-1} - \bar{p})^2$. Here, $a_0$ is a predisposition parameter capturing the possibility of autonomous switching, $a_x > 0$ is a herding parameter, $\bar{p}$ is the log fundamental value, and the misalignment parameter $a_d > 0$ governs the influence of price misalignment and the mean-reversion tendency, and thus introduces an asymmetry towards fundamentalism to the switching process. The implied population dynamics are as follows:

$$x'_t = x'_{t-1} + (1 - x'_{t-1})P_{t-1}^{c\to f} - (1 + x'_{t-1})P_{t-1}^{f\to c}. \tag{32}$$

The excess demand functions are given by:

$$\begin{cases} d_t^f = \phi(\bar{p} - p_t) + u_t^f, \\ d_t^c = \chi(p_t - p_{t-1}) + u_t^c, \end{cases} \tag{33}$$

where $\phi$ and $\chi$ are adjustment parameters for fundamentalists and chartists, respectively, and $u_t^f \sim N(0, \sigma_f^2)$ and $u_t^c \sim N(0, \sigma_c^2)$ are i.i.d. stochastic noise components of each of the demands. Finally, the implied log-price can be derived as:

$$p_t = p_{t-1} + \mu\left(\frac{1+x'_{t-1}}{2}\phi(\bar{p} - p_t) + \frac{1-x'_{t-1}}{2}\chi(p_t - p_{t-1}) + u_t\right), \tag{34}$$

where $\mu$ is a constant proportionality factor, and the noise term $u_t \sim N(0, \sigma_t^2)$ represents a structural stochastic volatility component of the model whose variance is governed by the population-weighted average of variances of $u_t^f$, $u_t^c$: $\sigma_t^2 = 0.5\big((1+x'_t)^2\sigma_f^2 + (1-x'_t)^2\sigma_c^2\big)$.

Parameters are set according to Franke and Westerhoff (2011) and summarized in Barde (2016) as follows: the flexibility parameter $\nu = 0.05$; the switching index parameters $a_0 = -0.155$, $a_x = 1.299$, and $a_d = 12.648$; the log fundamental value $\bar{p} = 0$; the adjustment parameter of the excess demands $\phi = 0.198$ and $\chi = 2.263$; the proportionality factor $\mu = 0.01$; and the standard deviations $\sigma_f = 0.782$ and $\sigma_c = 1.851$.

The flagship paper by Franke and Westerhoff (2012) build on their 2011 framework and present a model contest of structural stochastic volatility models focused on the replication capabilities of the important stylized facts and empirical moments within the estimation method of simulated moments. In addition to predisposition ($a_0$), herding ($a_x$), and price misalignment ($a_d$), they also consider a fourth principle that captures the discounted accumulated profits differential. The switching index is thus extended to the following general form: $s_t = a_0 + a_{x'}x'_{t-1} + a_d(p_{t-1} - \bar{p})^2 + a_w(w_{t-1}^f - w_{t-1}^c)$, where $a_w > 0$ can be interpreted as a wealth differential parameter because $w^f$ and $w^c$ denote the wealth of the fundamental and the characteristic strategies hypothetically accumulated over time. From 15 potential combinations of these four behavioral principles, the authors concentrate on and compare the four most relevant combinations under two switching approaches: the transition probability following the 2011 framework and the discrete choice approach following Brock and Hommes (1998). After an extensive model comparison via several criteria, the newly introduced wealth differential effect proves its ability to generate some interesting dynamics. However, the authors conclude that considering the moment coverage ratios criterion, the transition probability approach with predisposition, herding, and price misalignment behavioral principles *"happens to have found the best compromise in the trade-offs"* (pg. 1205), while on the grounds of minimizing the loss function that utilizes the joint coverage ratio, the contest winner is the discrete choice approach incorporating the same set of behavioral principles.

### *3.9. Schmitt and Westerhoff (2017) model with sunspots (SW)*

The latest model in our 'zoo' is an agent-based framework by Schmitt and Westerhoff (2017). The authors actually propose a simple large-scale model in which agents act according to their own individual rules but show that under suitable assumptions including a large number of agents, the large-scale version can be converted into a small-scale model. This computationally simplified approach, moreover, nests the 'winner' of the Franke and Westerhoff (2012) model contest, the discrete choice model with a predisposition, herding, and price misalignment behavioral principles. Since the model shares many common features with those by Franke and Westerhoff (2011) and Franke and Westerhoff (2012) described above, we would like to emphasize the main distinguishing ones: besides the notion of a large-scale agent-based framework in the background, the stochastic terms of the individual trading rules are not independent but multivariate-normally distributed with time-varying variance-covariance matrices. Potential situations of high correlation introduce into the model the rare occurrence of so-called sunspots, which might reflect e.g., a short-term influence by financial gurus or various exogenous events that may trigger an extreme event.

The computational version analyzed in this study is the 'S-CF model' in which both fundamentalists and chartists obtain sunspots. The price adjustment process follows the following equation:

$$\begin{aligned} P_t = P_{t-1} + a^M(W_{t-1}^C a^C(P_{t-1} - P_{t-2}) + s^C\sqrt{W_{t-1}^C}\sqrt{1 + X_{t-1}^C W_{t-1}^C}\,\varepsilon_{t-1}^C \\ + (1 - W_{t-1}^C)a^F(F - P_{t-1}) + s^F\sqrt{1 - W_{t-1}^C}\sqrt{1 + X_{t-1}^F(1 - W_{t-1}^C)}\,\varepsilon_{t-1}^F), \end{aligned} \tag{35}$$

where $P_t$ is the log price of the risky asset at time $t$, $a^M > 0$ denotes the market maker's price adjustment parameter, $W^C$ is the relative number of chartists to fundamentalists defined in (37), $\{a^C > 0,\ s^C > 0\}$ and $\{a^F > 0,\ s^F > 0\}$ are the mean and the variance scaling coefficient pairs for the individual trend extrapolation or the individual price misalignment reaction parameters, respectively, and $\{X^C, X^F\}$ defined in (36) relate to the elements $\{\rho^C, \rho^F\}$ of the time-varying variance-covariance matrices as $\rho^C = X^C/N$, in which $N$ is the total number of agents and

$$\begin{cases} X_{t-1}^C = \begin{cases} X^{C,h} \text{ with probability } S^C \\ X^{C,l} \text{ with probability } 1 - S^C, \end{cases} \\ X_{t-1}^F = \begin{cases} X^{F,h} \text{ with probability } S^F \\ X^{F,l} \text{ with probability } 1 - S^F, \end{cases} \end{cases} \tag{36}$$

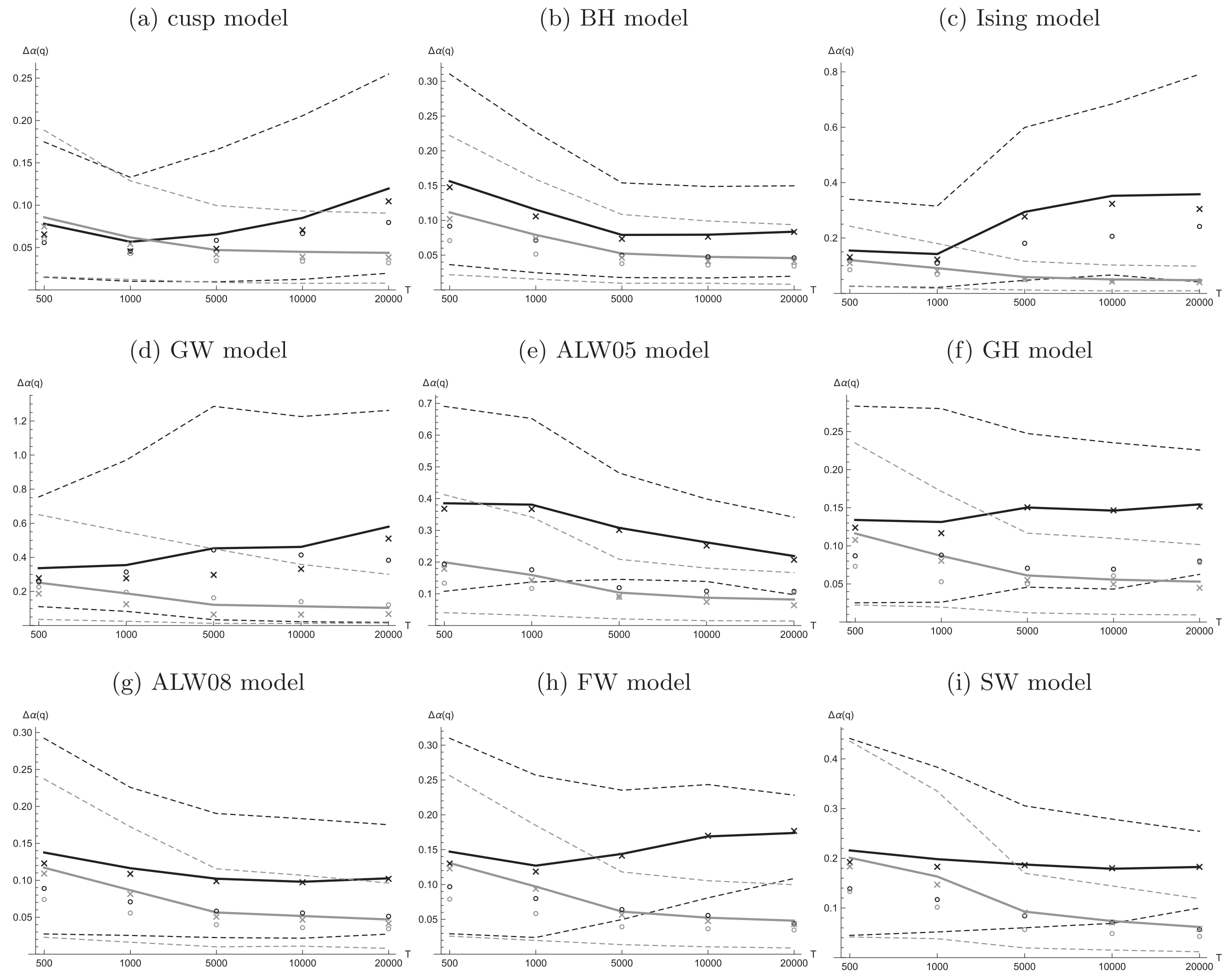


**Fig. 3.** Results for the MF-DFA $\Delta\alpha(q)$ estimation. *Note:* The vertical axis shows the estimated values; the horizontal axis shows the lengths $T$ of the time series. Black color represents results for the original series and gray color for the randomly shuffled series. Results are based on 1,000 random runs. Unbroken bold lines depict sample means of estimated values, and the ' × ' symbols display sample medians. Dashed thin lines depict 5% and 95% quantiles, and the '○' symbols display the sample standard errors.

where $X^{C,h}$, $X^{C,l}$, $X^{F,h}$, $X^{F,l}$ are the higher and lower boundary parameters, and $\{S^C, S^F\}$ are the probabilities of a sunspot case occurrence for chartists and fundamentalists, respectively. Finally, $F$ stands for the log price of the risky asset, $\varepsilon_t^C \sim N(0,1)$, $\varepsilon_t^F \sim N(0,1)$, and the market share of chartists follows:

$$W_{t-1}^C = \frac{1}{1+\exp\left(\gamma[b^0 + b^H(1-2W_{t-2}^C) + b^M(F-P_{t-2})^2]\right)}, \tag{37}$$

where $\gamma$ is a homogeneous intensity of choice for all agents, and $b^0$, $b^H$, and $b^M$ are the homogeneous predisposition, herding, and price misalignment parameters, respectively.

The computational design follows the (Schmitt and Westerhoff, 2017, Table 2, S-CF, Fig. 5) setup with $a^M = 0.01,\ a^C = 1.5,\ a^F = 0.138,\ s^C = 1.653,\ s^F = 0.545,\ F = 0;\ X^{C,h} = 20,\ X^{F,h} = 40,\ X^{C,l} = X^{F,l} = 0,\ S^C = 0.009,\ S^F = 0.005;\ \gamma = 1,\ b^0 = -0.336,\ b^H = 2.446,\ b^M = 19.671.$

## 4. Numerical study

### 4.1. Simulation setup

This section describes a general setup for all individual numerical exercises if not explicitly stated otherwise. Computations are conducted using R. The computational burden has been made manageable taking advantage of the parallel server capacities while utilizing the doParallel and the foreach packages that execute for-loop iterations in parallel (alternatively, the parallel package and the parApply family of functions can be used). The specific calibration for each model from Section 3 is always based on the original paper introducing the model or a follow-up research contribution providing a benchmark setup. The calibration details for each model are specified in Section 3.

A Monte Carlo study aggregating outputs over 1000 random runs for each estimation setup ensures the statistical validity of the results. Five different lengths of model output time series ($T = 500,\ 1,000,\ 5,000,\ 10,000,\ 20,000$) are studied, and a sufficient number of additional observations are always discarded as a burn-in period to eliminate potential influence of the random initial conditions for each run. To distinguish whether a potential multifractality is due to an agent-based correlation structure of the model or distributional properties of the underlying process, we standardly compare the results based on the original series with the results based on a randomly shuffled series. Shuffling is always performed by taking the original series and mixing randomly all its single observations. This procedure ensures a complete deterioration of any autocorrelation structures.

With respect to the multifractality estimation setup, we set the maximum moment order to $q_{max} = 3$, the minimum moment order $q_{min} = -q_{max}$, with a step of $q_{step} = 1$ for MF-DFA and MF-DMA. For the GHE, $q_{min,GHE} = 0.1$, and $q_{step,GHE} = 0.1$. We also experimented with $q_{max} = \{4, 5, 10\}$, bringing negligible additional information for the results while increasing the computational costs markedly.[3]

*4.2. General findings*

For each model, we graphically depict a set of aggregate descriptive statistics for all three methods for estimation of the multifractal metrics specified in Section 2.2 and for both $\Delta\alpha(q)$ and $\Delta H(q)$: the mean, the median, 5% and 95% quantiles, and the sample standard error. Figs. 3 to A.10 summarize the aggregated outcomes of our analysis.

The first important finding suggests that both $\Delta\alpha(q)$ and $\Delta H(q)$ metrics provide particularly similar knowledge if Figs. 3 and A.7, 4 and A.8, and A.9 and A.10 are compared pairwise. The only difference lies in the scale of the vertical axis of individual graphs, where for both MF-DFA and MF-DMA, $\Delta\alpha(q)$ displays larger absolute values of displayed estimates, while the relative proportions of the estimated values for the original vs. the shuffled series are not much affected. The second important finding is that while both MF-DFA and MF-DMA provide contributive results suggesting strong multifractal features for some models due to an agent-based correlation structure and, on the other hand, rejecting an interesting multifractal structure for other models, the GHE-based estimation method provides generally poor and counterintuitive results. For instance, for most of analyzed models in Figs. A.9 and A.10, the mean of estimates of the GHE for the randomly shuffled series (gray) is larger than for the original series (black), which is a puzzling numerical result without a clear theoretical rationale. For the remaining models, the results for the original (black) and the shuffled (gray) series are largely identical, calling into question the reliability of the GHE estimation method. The observed bias of the results for the shuffled series can come from even a small negative serial correlation (see Barunik et al., 2012 for discussions) contrasted with results of the standardly used MF-DFA. This result can be explained, e.g., by various forms of mean-reverting tendencies that usually characterize financial agent-based models. Interestingly, the results for the Ising model largely differ for $\Delta\alpha(q)$ and $\Delta H(q)$ based on the GHE estimation, adding one additional puzzling question to the discussion about the reliability of this method.

By virtue of the abovementioned findings, we finally follow with a detailed interpretation of Figs. 3 and 4 showing $\Delta\alpha(q)$ estimates for MF-DFA and MF-DMA, as these two effectively contain all important results of our analysis. Other depicted results are relegated to the Appendix.

*4.2.1. Detection of multifractality*

We conclude that a given model generates interesting multifractal patterns due to an agent-based correlation structure if two criteria are met. First, the mean of estimated $\Delta\alpha(q)$ of the original series (black) is generally increasing in the length $T$ of the analyzed time series depicted on the horizontal axis because a longer dataset provides a higher potential to detect multifractality. An exception might be observed for the shortest datasets of $T = 500$ or $1,000$ observations, where the lack of data might cause significant bias of the estimator. Second, we need to observe a considerably higher mean of the estimated $\Delta\alpha(q)$ for the original series (black) than for shuffled series (gray). Optimally, this difference is increasing in the length $T$ of the analyzed time series and statistically significant at the given confidence level for large $T$, i.e., the two estimated metrics diverge. The multifractality is then clearly due to a complex agent-based design of the model because in the randomly shuffled series (gray), the correlation links originating in the data generation process of agents' interactions and evolution of market fractions are broken.

*4.2.2. Results for specific models*

Five models clearly fit the above-specified criteria: the Ising model and the GW, GH, FW, and SW models. Moreover, for the FW model, an important supplementary criterion of a statistically significant difference demonstrated by the disconnected 90% sample confidence intervals of $\Delta\alpha(q)$ for the original (black) and the shuffled (gray) series can be observed in

[3] Interestingly, with increasing $q_{max}$, we do not necessarily obtain a higher multifractality detection performance for some models. A potential explanation for this seemingly counterintuitive phenomenon is that financial agent-based models produce time series with both interesting correlation structures and heavy tails that naturally cannot be eliminated with shuffling. Higher $q_{max}$ then can accentuate the heavy tails more than the multifractal correlation structures, which might result in actually lower $\Delta\alpha(q)$ and $\Delta H(q)$ compared to the lower $q_{max}$.

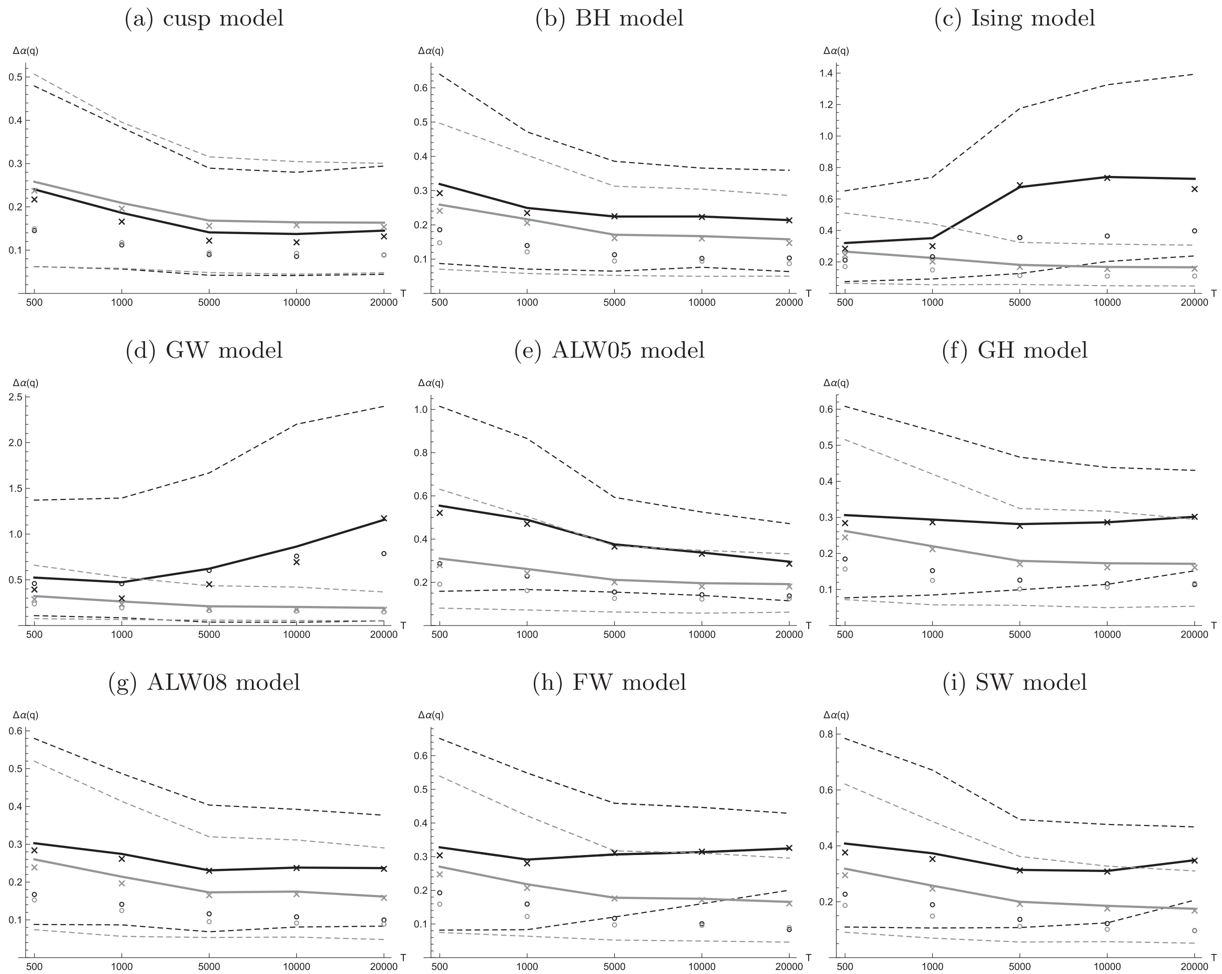


**Fig. 4.** Results for the MF-DMA $\Delta\alpha(q)$ estimation. *Note:* The vertical axis shows the estimated values; the horizontal axis shows the lengths $T$ of the time series. Black color represents results for the original series and gray color for the randomly shuffled series. Results are based on 1,000 random runs. Unbroken bold lines depict sample means of estimated values, and the ' $\times$ ' symbols display sample medians. Dashed thin lines depict 5% and 95% quantiles, and the '$\circ$' symbols display the sample standard errors.

Fig. 3 for MF-DFA with the length of $T = 20,000$ observations. A similar asymptotic tendency can be observed also for the GH and SW models and in Fig. 4 additionally for the Ising model for the MF-DMA estimation method.

On the other hand, for the BH model, none of the criteria seems convincingly satisfied, and we thus conclude that no interesting multifractal structures can be detected in the generated time series. Results for the three remaining models are somewhat puzzling. The cusp model satisfies the two criteria only based on the MF-DFA estimation. For the MF-DMA, the results actually suggest a completely opposite behavior, that is, no interesting multifractal features at all. We double-checked this ambiguous finding to confirm it is a feature and not a bug, and it also remains robust w.r.t. various calibration setups of the model. The ALW05 model displays a partially puzzling behavior when estimated using both methods. The second criterion of a considerably higher $\Delta\alpha(q)$ estimates is satisfied particularly for the MF-DFA estimation, but the difference is decreasing in the length $T$ of the analyzed time series as well as is the mean of estimated $\Delta\alpha(q)$. Therefore, the two estimated metrics appear to slowly converge with one another suggesting that there is no gain in terms of the multifractal structure from a complex agent-based correlation structure of the model. The ALW08 model somewhat satisfies both criteria based on the MF-DFA estimation but for the MF-DMA, the mean of estimated $\Delta\alpha(q)$ of the original series (black) is rather decreasing or stable and the difference w.r.t. the shuffled series (gray) seems stable as well.

### 4.2.3. Additional interpretations for multifractal models

For the five models with prospective multifractal features, that is, the Ising, GW, GH, FW, and SW models, we interpret additional results observable in Figs. 3 and 4. In this section, we further focus only on the results related to the original series (black).

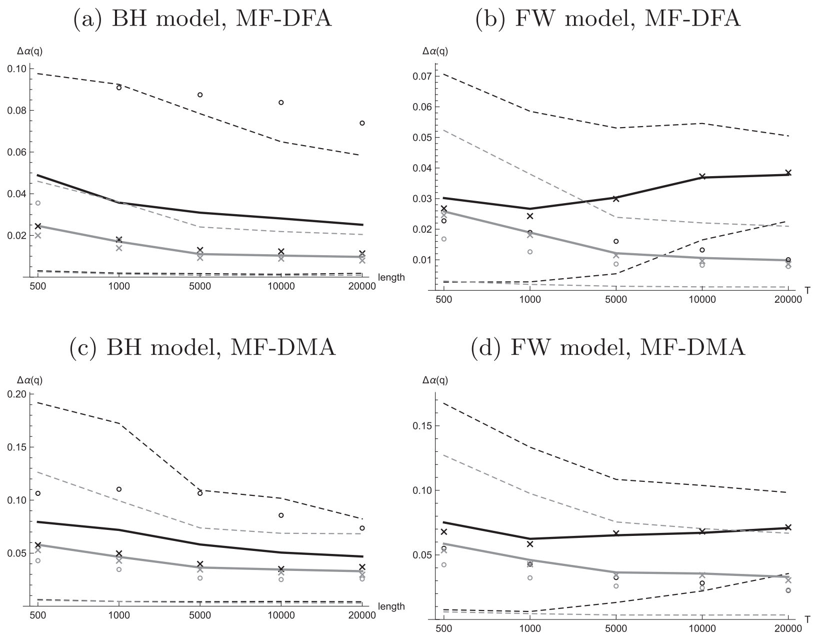


**Fig. 5.** Validity check I—$\Delta\alpha(q)$ estimation with $q_{max} = -q_{min} = 1$. *Note:* The vertical axis shows the estimated values; the horizontal axis shows the lengths $T$ of the time series. Black color represents results for the original series and gray color for the randomly shuffled series. Results are based on 1,000 random runs. Unbroken bold lines depict sample means of estimated values, and the ‘ × ’ symbols display sample medians. Dashed thin lines depict 5% and 95% quantiles, and the ‘○’ symbols display the sample standard errors.

Primarily, to rigorously evaluate the second criterion, we compute exact ratios of the mean of $\Delta\alpha(q)$ estimates between the original and the shuffled series for the length $T = 20,000$ observations estimated via MF-DFA: 7.52 (Ising), 5.59 (GW), 3.62 (FW), 2.95 (SW), 2.91 (GH); and via MF-DMA: 5.99 (GW), 4.39 (Ising), 1.99 (SW), 1.96 (FW), 1.76 (GH). These ratios can serve as quantification of multifractality for each given model. Interestingly, focusing now on the first criterion, while the $\Delta\alpha(q)$ estimates for the original series (black) suggest an approximately linearly increasing multifractality for the GW and FW models when comparing results for larger samples ($T = 5,000,\ 10,000,\ 20,000$), the GH and SW models exhibit rather constant behavior, and the Ising model clearly displays a marginally decreasing growth.

Second, the sampling distribution of the $\Delta\alpha(q)$ estimator appears to be right (positively) skewed for the Ising and GW model, as sample medians (‘ × ’ symbol) are generally below the mean values. This feature is very evident in the case of the MF-DFA estimation but to a large extent disappears for the MF-DMA. Second, the variance of the estimator for the Ising and the GW models is rather large, as can be observed either from the 90% sample confidence intervals or the sample standard errors (‘○’ symbol). Moreover, it is either increasing or remains relatively stable for the Ising, GW, and GH models in the length $T$ of the analyzed time series. Conversely, the results for the GH, FW, and SW models suggest no skewness of the estimator, and for the FW and SW models also a decreasing tendency of the variance, which can be observed from both the decreasing sample standard errors and the narrowing 90% sample confidence intervals. As already highlighted above, for MF-DFA and the length of 20,000 observations, for the FW model we observe an important disconnection of the 90% sample confidence intervals of $\Delta\alpha(q)$ between the original and the shuffled series. This finding can be translated to an econometric inference of a statistically different $\Delta\alpha(q)$ based on the given confidence level.

### *4.3. Validity checks*

Possible imperfections of our findings can potentially come from a partially artificially estimated multifractality based on a specific computational setup. We, therefore, assure the validity of the presented results by two checks. First (I), we follow the conservative approach suggested by Morales et al. (2012) and Buonocore et al. (2017) when setting the interval for the moment order $q$. The maximum and minimum moment orders are therefore set as $q_{max} = -q_{min} = 1$ instead of $q_{max} = -q_{min} = 3$ as the first validity check. Second (II), to assure the validity of the multifractality estimation due to an agent-based correlation structure of the model, we repeatedly randomly shuffle the original series and depict the sample averages of the measured sample moments based on 10 randomizations instead of a single shuffling.

Our results prove completely robust in both validity checks. As a representative illustration of the robustness, we depict in Fig. 5 an example of the MF-DFA $\Delta\alpha(q)$ estimation for two models selected based on the previous analysis, one

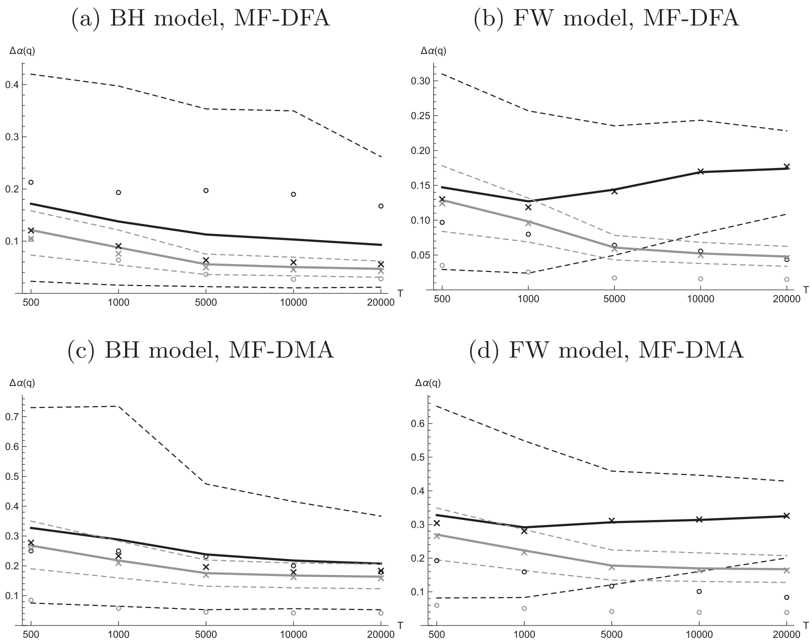


**Fig. 6.** Validity check II—$\Delta\alpha(q)$ estimation with 10 random shufflings. *Note:* The vertical axis shows the estimated values; the horizontal axis shows the lengths $T$ of the time series. Black color represents results for the original series and gray color for the randomly shuffled series. Results are based on 1,000 random runs. Unbroken bold lines depict sample means of estimated values, and the ' $\times$ ' symbols display sample medians. Dashed thin lines depict 5% and 95% quantiles, and the '$\circ$' symbols display the sample standard errors.

without interesting multifractal behavior and the other generating strong multifractal patterns, i.e., the Brock and Hommes (1998) model and the Franke and Westerhoff (2011) model, respectively. Fig. 5 shows the results for the maximum and minimum moment orders $q_{max} = -q_{min} = 1$ and can be directly compared to Figs. 3 and 4, panels (b) and (h). Qualitatively, one can observe an almost unchanged behavior for both models even after the restriction, though the variance of the estimator considerably increases for the BH model. Naturally, the width of the multifractal spectrum on the vertical axis is much smaller for lower $q_{max}$. Fig. 6 shows the results for 10 randomizations of the shuffling of the original series and can be compared similarly. Again, the robustness of the original results can be clearly observed from a comparison with Figs. 3 and 4, panels (b) and (h), as the overall behavior keeps generally unchanged. The multiple randomization improves results especially for the FW model as it naturally refines estimates for the shuffled series and hence considerably narrows the related 90% sample confidence intervals.

## 5. Conclusion

Agent-based models are usually claimed to generate complex dynamics; however, the link to such complexity has not been put to a more rigorous examination. We, therefore, study multifractality as a measure of complexity and a new stylized fact of financial time series that can be replicated by some of the small-scale financial agent-based models. The paper thus analyzes the link between the complexity of financial time series—measured by their multifractal properties—and the design of various agent-based frameworks used to model the heterogeneity of financial markets.

Nine popular elementary financial agent-based models are analyzed in terms of the multifractal properties of the generated time series. The list of the 'model zoo' begins with one of the oldest small-scale models in the literature introducing the concept of behavioral heterogeneity among financial market participants, the cusp catastrophe model by Zeeman (1974); and ends with one of the most recent approaches by Schmitt and Westerhoff (2017) that is a computationally simplified version of a large-scale 'structural volatility' model with mutually dependent individual stochastic terms and the occurrence of sunspots that may trigger extreme events. Our choice is driven by an effort to encompass various types of modeling approaches and mechanisms triggering endogenous evolutionary dynamics. In an extensive Monte Carlo simulation analysis, we utilize the toolkit of MF-DFA, MF-DMA, and GHE-based estimators of the range of $\Delta H(q)$ and the width of the spectrum $\Delta\alpha(q)$, which are considered natural measures of multifractality.

We find that while both the $\Delta\alpha(q)$ and $\Delta H(q)$ metrics provide particularly similar and contributive results suggesting interesting multifractal features for some models due to an agent-based correlation structure, the GHE-based estimator provides generally poor and counterintuitive results, calling into question the reliability of the estimation method. Five models meet the two criteria specified to detect multifractal behavior: the Bornholdt (2001) Ising model, and the Gilli and Winker (2003) (GW), Gaunersdorfer and Hommes (2007) (GH), Franke and Westerhoff (2011) (FW), and Schmitt and Westerhoff (2017) (SW) models. Moreover, an important supplementary criterion of a statistically significant difference demonstrated by the disconnected 90% sample confidence intervals of $\Delta\alpha(q)$ for the original and the shuffled series holds for the FW model. A similar asymptotic tendency can be observed also for the GH and SW models. Finally, for the FW and SW models, the $\Delta\alpha(q)$ estimators display a decreasing tendency of the variance.

We also precisely compute exact ratios of the mean of the $\Delta\alpha(q)$ estimates between the original and the shuffled series that can serve as a direct quantification of multifractality due to the correlation structure. Moreover, while results for the GW and FW models show an approximately linearly increasing multifractality with the length of time series, the GH and SW models exhibit rather constant behavior, and the Ising model clearly displays a marginally decreasing growth. Next, especially the MF-DFA estimator of $\Delta\alpha(q)$ appears right-skewed for the Ising and GW models, and it also exhibits high and generally stable or increasing variance. Conversely, the results for the GH, FW, and SW models suggest no skewness of the estimator, and for the FW and SW models also a decreasing tendency of the variance, leading to an important disconnection of the 90% sample confidence intervals of $\Delta\alpha(q)$ between the original and the shuffled series for large datasets. The results prove robust w.r.t. a set of validity checks. We thus suggest that the presence of multifractality can potentially be used as one of the new means of validation of financial agent-based models.

On the other hand, for the Brock and Hommes (1998) (BH) model, none of the multifractal behavior criteria seems convincingly satisfied and we thus conclude that no interesting multifractal structures can be detected in the generated time series. A closer look might be useful for the cusp (Zeeman, 1974) and the Alfarano et al. (2005, 2008) models, where results display somewhat puzzling behavior. Complexity is thus not an automatic feature of the time series generated by any financial agent-based model but only the models with specific properties.

Future research on the main sources of complex dynamics can proceed further to a sensitivity analysis of the coherence of multifractal estimates by varying the structural design of the multifractal financial agent-based models. It can focus, for instance, on the assessment of whether and how the multifractal properties of the time series generated by multifractal models react to changes in essential model parameters. Specific attention can also be devoted to the general impact of robust qualitative principles triggering model dynamics. Following Franke (2010) and Franke and Westerhoff (2012), an important topic to study is the link between various sources and definitions of the stochastic noise in these models and their complexity. Additionally, a broader question regards the impact of the leading switching mechanism on the multifractal properties of financial agent-based models.

## Acknowledgments

We gratefully acknowledge financial support from the Czech Science Foundation under the 17-12386Y 'Multifractality analysis in finance' project and from the Charles University PRIMUS program [project PRIMUS/19/HUM/17]. Kukacka gratefully acknowledges financial support from the Charles University UNCE program [project UNCE/HUM/035]. The MATLAB code of the ALW08 model has been kindly provided by Prof. Thomas Lux (University of Kiel, Germany) and Dr. Zhenxi Chen (South China University of Technology). The MATLAB codes of the GW, ALW05, and FW models have been kindly provided by Dr. Sylvain Barde (University of Kent, UK). The Mathematica code of the SW model have been kindly provided by Prof. Frank Westerhoff (University of Bamberg, Germany). The MATLAB code of the GH model has been downloaded from the agentFin 0.1 documentation web page [accessed 2019-10-28] by Prof. Blake LeBaron (Brandeis University, USA). This paper has benefited from discussions with Giuseppe Brandi and participants at the 23rd and 24th Annual Workshops on Economic Science with Heterogeneous Interacting Agents in Tokyo (2018) and London (2019). Finally, we are very thankful to the two anonymous reviewers for their inspiring comments and detailed suggestions.

## Appendix A

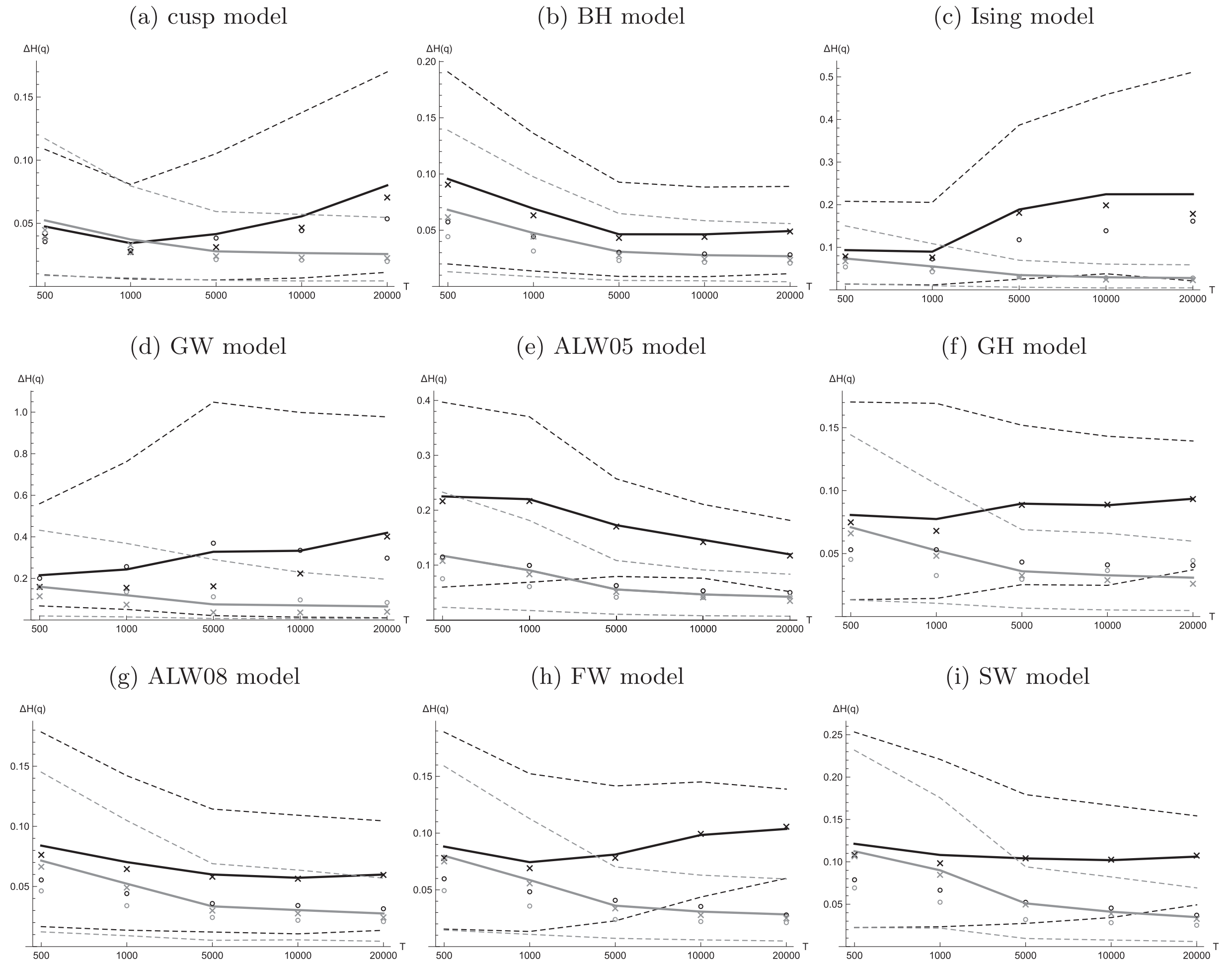


**Fig. 7.** Results for the MF-DFA $\Delta H(q)$ estimation. *Note:* The vertical axis shows the estimated values; the horizontal axis shows the lengths $T$ of the time series. Black color represents results for the original series and gray color for the randomly shuffled series. Results are based on 1,000 random runs. Unbroken bold lines depict sample means of estimated values, and the ' $\times$ ' symbols display sample medians. Dashed thin lines depict 5% and 95% quantiles, and the '$\circ$' symbols display the sample standard errors.

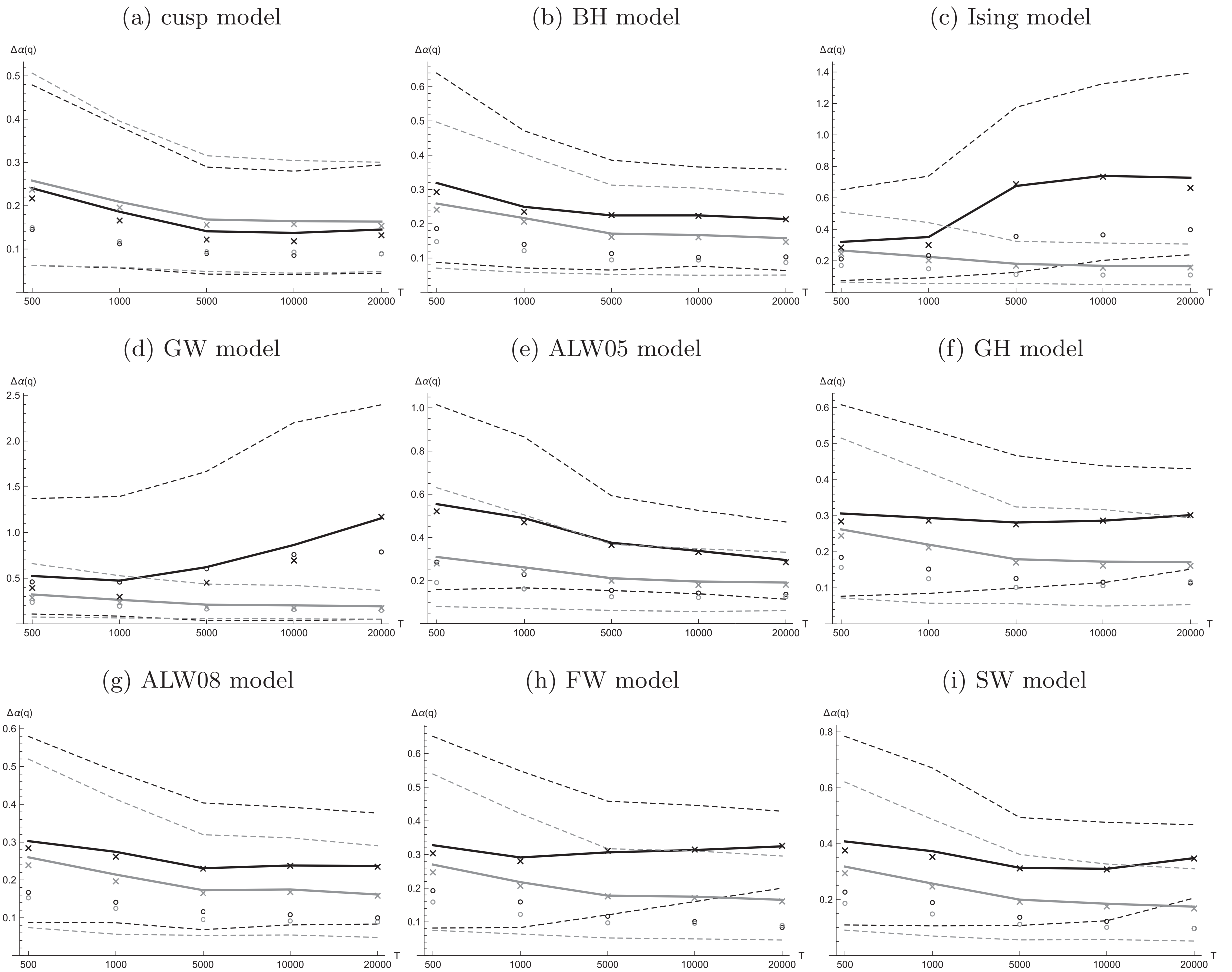


**Fig. 8.** Results for the MF-DMA $\Delta H(q)$ estimation. *Note:* The vertical axis shows the estimated values; the horizontal axis shows the lengths $T$ of the time series. Black color represents results for the original series and gray color for the randomly shuffled series. Results are based on 1,000 random runs. Unbroken bold lines depict sample means of estimated values, and the ' × ' symbols display sample medians. Dashed thin lines depict 5% and 95% quantiles, and the '∘' symbols display the sample standard errors.

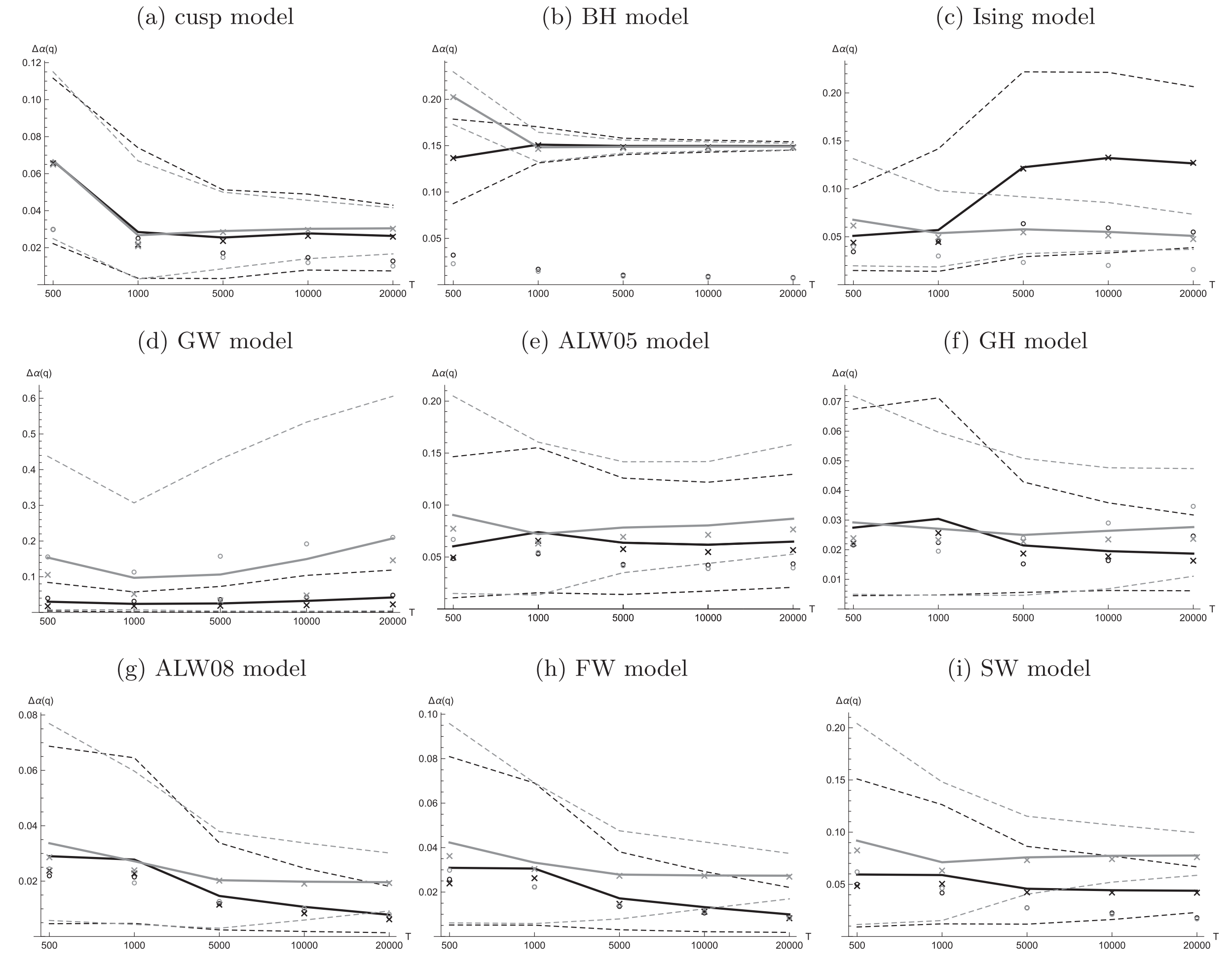


**Fig. 9.** Results for the GHE $\Delta\alpha(q)$ estimation. *Note:* The vertical axis shows the estimated values; the horizontal axis shows the lengths *T* of the time series. Black color represents results for the original series and gray color for the randomly shuffled series. Results are based on 1,000 random runs. Unbroken bold lines depict sample means of estimated values, and the ' $\times$ ' symbols display sample medians. Dashed thin lines depict 5% and 95% quantiles, and the '$\circ$' symbols display the sample standard errors.

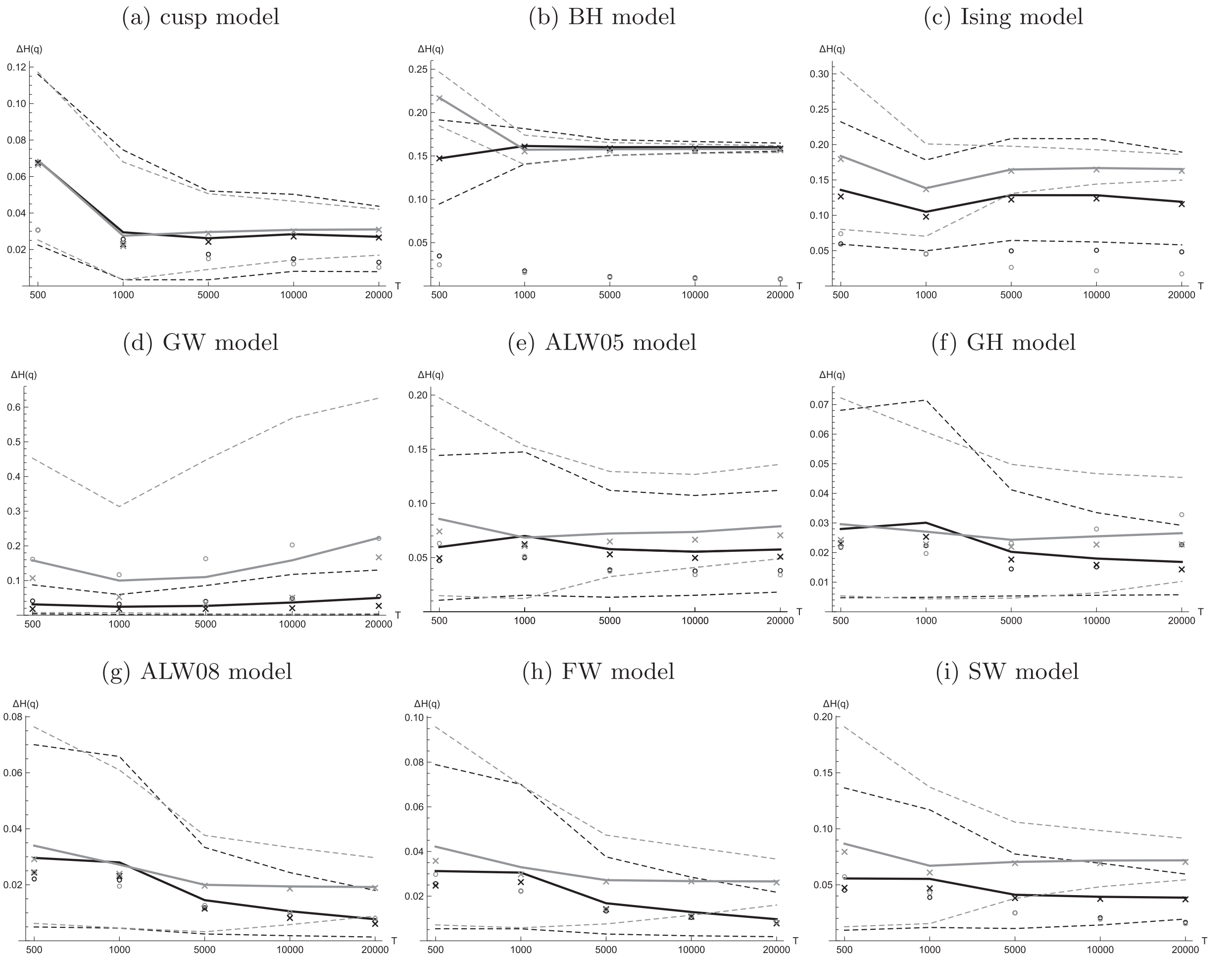


**Fig. 10.** Results for the GHE $\Delta H(q)$ estimation. *Note:* The vertical axis shows the estimated values; the horizontal axis shows the lengths $T$ of the time series. Black color represents results for the original series and gray color for the randomly shuffled series. Results are based on 1,000 random runs. Unbroken bold lines depict sample means of estimated values, and the ' × ' symbols display sample medians. Dashed thin lines depict 5% and 95% quantiles, and the '○' symbols display the sample standard errors.

## Supplementary material

Supplementary material associated with this article containing R codes for the estimators of the generalized Hurst exponent (MF-DFA, MF-DMA, and GHE methods), R code and empirical data used in Section 2.3, and three illustrative examples of the estimation procedure can be found, in the online version, at doi: 10.1016/j.jedc.2020.103855.

## References


Alessio, E., Carbone, A., Castelli, G., Frappietro, V., 2002. Second-order moving average and scaling of stochastic time series. Eur. Phys. J. B 27, 197–200.
Alfarano, S., Lux, T., Wagner, F., 2005. Estimation of agent-based models: the case of an asymmetric herding models. Comput. Econ. 26, 19–49.
Alfarano, S., Lux, T., Wagner, F., 2008. Time variation of higher moments in a financial market with heterogeneous agents: an analytical approach. J. Econ. Dyn. Control 32 (1), 101–136.
Amilon, H., 2008. Estimation of an adaptive stock market model with heterogeneous agents. J. Empir. Financ. 15 (2), 342–362.
Arneodo, A., Decoster, N., Roux, S., 2000. A wavelet-based method for multifractal image analysis. I. Methodology and test applications on isotropic and anisotropic random rough surfaces. Eur. Phys. J. B 15 (3), 567–600.
Ashkenazy, Y., Baker, D., Gildor, H., Havlin, S., 2003. Nonlinearity and multifractality of climate change in the past 420,000 years. Geophys. Res. Lett. 30 (22), 2146.
Bacry, E., Kozhemyak, A., Muzy, J.F., 2008. Continuous cascade models for asset returns. J. Econ. Dyn. Control 32 (1), 156–199.
Barde, S., 2016. Direct comparison of agent-based models of herding in financial markets. J. Econ. Dyn. Control 73, 329–353.
Barunik, J., Aste, T., Matteo, T.D., Liu, R., 2012. Understanding the source of multifractality in financial markets. Phys. A Stat. Mech. Appl. 391 (17), 4234–4251.
Barunik, J., Kukacka, J., 2015. Realizing stock market crashes: stochastic cusp catastrophe model of returns under time-varying volatility. Quant. Financ. 15 (6), 959–973.
Beran, J., 1994. Statistics for long-memory processes. In: Monographs on Statistics and Applied Probability, Vol. 61. Chapman and Hall, New York:.
Bornholdt, S., 2001. Expectation bubbles in a spin model of markets: Intermittency from frustration across scales. Int. J. Mod. Phys. C 12 (5), 667–674.
Brock, W.A., Hommes, C.H., 1998. Heterogeneous beliefs and routes to chaos in a simple asset pricing model. J. Econ. Dyn. Control 22, 1235–1274.
Buonocore, R.J., Aste, T., Matteo, T.D., 2016. Measuring multiscaling in financial time-series. Chaos Solitons Fractals 88, 38–47.
Buonocore, R.J., Aste, T., Matteo, T.D., 2017. Asymptotic scaling properties and estimation of the generalized hurst exponents in financial data. Phys. Rev. E 95, 042311.
Calvet, L., Fisher, A., 2001. Forecasting multifractal volatility. J. Econom. 105 (1), 27–58.
Calvet, L., Fisher, A., 2002. Multifractality in asset returns: theory and evidence. Rev. Econ. Stat. 84, 381–406.
Chechkin, A., Gonchar, V., 2000. Self and spurious multi-affinity of ordinary Levy motion, and pseudo-Gaussian relations. Chaos Solitons Fractals 11 (14), 2379–2390.
Chen, S.-H., Chang, C.-L., Du, Y.R., 2012. Agent-based economic models and econometrics. Knowl. Eng. Rev. 27, 187–219. 6
Chen, Z., Lux, T., 2018. Estimation of sentiment effects in financial markets: a simulated method of moments approach. Comput. Econ. 52 (3), 711–744.
Cobb, L., 1981. Parameter estimation for the cusp catastrophe model. Behav. Sci. 26 (1), 75–78.
Cont, R., 2001. Empirical properties of asset returns: stylized facts and statistical issues. Quant. Financ. 1 (2), 223–236.
Cont, R., Bouchaud, J.P., 2000. Herd behavioor and aggregate fluctuations in financial markets. Macroecon. Dyn. 4 (2), 170.196.
Cont, R., Teyssiere, G., Kirman, A., 2007. Volatility clustering in financial markets: empirical facts and agent-based models. In: Long Memory in Economics. Springer Berlin Heidelberg, pp. 289–309.
Dellino, P., Liotino, G., 2002. The fractal and multifractal dimension of volcanic ash particles contour: a test study on the utility and volcanological relevance. J. Volcanol. Geotherm. Res. 113 (1-2), 1–18.
Di Matteo, T., 2007. Multi-scaling in finance. Quant. Financ. 7 (1), 21–36.
Di Matteo, T., Aste, T., Dacorogna, M., 2003. Scaling behaviors in differently developed markets. Phys. A Stat. Mech. Appl. 324, 183–188.
Di Matteo, T., Aste, T., Dacorogna, M., 2005. Long-term memories of developed and emerging markets: using the scaling analysis to characterize their stage of development. J. Bank. Financ. 29, 827–851.
Fagiolo, G., Guerini, M., Lamperti, F., Moneta, A., Roventini, A., 2019. Validation of Agent-Based Models in Economics and Finance. Springer International Publishing, pp. 763–787.
Franke, R., 2010. On the specification of noise in two agent-based asset pricing models. J. Econ. Dyn. Control 34 (6), 1140–1152.
Franke, R., Westerhoff, F., 2011. Estimation of a structural stochastic volatility model of asset pricing. Comput. Econ. 38 (1), 53–83.
Franke, R., Westerhoff, F., 2012. Structural stochastic volatility in asset pricing dynamics: estimation and model contest. J. Econ. Dyn. Control 36 (8), 1193–1211.
Franke, R., Westerhoff, F., 2016. Why a simple herding model may generate the stylized facts of daily returns: explanation and estimation. J. Econ. Interact. Coord. 11 (1), 1–34.
Frankel, J.A., Froot, K.A., 1986. Understanding the us dollar in the eighties: the expectations of chartists and fundamentalists. Econ. Record 24–38.
Gaunersdorfer, A., Hommes, C., 2007. A Nonlinear Structural Model for Volatility Clustering. Springer Berlin Heidelberg, Berlin, Heidelberg:, pp. 265–288.
Gaunersdorfer, A., Hommes, C.H., Wagener, F.O., 2008. Bifurcation routes to volatility clustering under evolutionary learning. J. Econ. Behav. Organ. 67 (1), 27–47.
Ghonghadze, J., Lux, T., 2016. Bringing an elementary agent-based model to the data: estimation via GMM and an application to forecasting of asset price volatility. J. Empir. Financ. 37, 1–19.
Gilli, M., Winker, P., 2003. A global optimization heuristic for estimating agent based models. Comput. Stat. Data Anal. 42, 299–312.
Grazzini, J., Richiardi, M., 2015. Estimation of ergodic agent-based models by simulated minimum distance. J. Econ. Dyn. Control 51, 148–165.
Grech, D., Pamuła, G., 2012. Multifractal background noise of monofractal signals. Acta Phys. Polon. A 121 (2), B34–B39.
Grech, D., Pamuła, G., 2013. On the multifractal effects generated by monofractal signals. Phys. A Stat. Mech. Appl. 392 (23), 5845–5864.
Hommes, C.H., Tesfatsion, L., Judd, K., 2006. Chapter 23: heterogeneous agent models in economics and finance. In: Handbook of Computational Economics, 2. Elsevier, pp. 1109–1186.
Hu, W., Wen, G., Rahmani, A., Yu, Y., 2019. Distributed consensus tracking of unknown nonlinear chaotic delayed fractional-order multi-agent systems with external disturbances based on ABC algorithm. Commun. Nonlinear Sci. Numer. Simul. 71, 101–117.
Jiang, Z.-Q., Xie, W.-J., Zhou, W.-X., Sornette, D., 2018. Multifractal analysis of financial markets. Technical report.
Jiang, Z.-Q., Zhou, W.X., 2011. Multifractal detrending moving-average cross-correlation analysis. Phys. Rev. E 84, 016106.
Kantelhardt, J., 2009. Encyclopedia of complexity and systems science. In: Chapter Fractal and Multifractal Time Series. Springer-Verlag New York, pp. 3754–3779.
Kantelhardt, J., Zschiegner, S., Koscielny-Bunde, E., Bunde, A., Havlin, S., Stanley, E., 2002. Multifractal detrended fluctuation analysis of nonstationary time series. Phys. A Stat. Mech. Appl. 316 (1-4), 87–114.
Kirman, A., 1991. Money and financial markets. In: Chapter Epidemics of Opinion and Speculative Bubbles in Financial Markets. Macmillan, New York, USA., pp. 354–368.
Kirman, A., 1993. Ants, rationality, and recruitment. Q. J. Econ. 108 (1), 137–156.
Kristoufek, L., Vosvrda, M., 2018. Herding, minority game, market clearing and efficient markets in a simple spin model framework. Commun. Nonlinear Sci. Numer. Simul. 54, 148–155.

Kukacka, J., Barunik, J., 2013. Behavioural breaks in the heterogeneous agent model: the impact of herding, overconfidence, and market sentiment. Phys. A Stat. Mech. Appl. 392 (23), 5920–5938.
Kukacka, J., Barunik, J., 2017. Estimation of financial agent-based models with simulated maximum likelihood. J. Econ. Dyn. Control 85, 21–45.
LeBaron, B., Tesfatsion, L., 2008. Modeling macroeconomies as open-ended dynamic systems of interacting agents. Am. Econ. Rev. 98 (2), 246–250.
Liu, R., Matteo, T.D., Lux, T., 2007. True and apparent scaling: the proximity of the Markov-switching multifractal model to long-range dependence. Phys. A Stat. Mech. Appl. 383 (1), 35–42. Econophysics Colloquium 2006 and Third Bonzenfreies Colloquium
Lopes, R., Betrouni, N., 2009. Fractal and multifractal analysis: a review. Med. Image Anal. 13 (4), 634–649.
Lucas, R.E.J., 1978. Asset prices in an exchange economy. Econometrica 46, 1429–1445.
Lux, T., 2008. Stochastic behavioral asset pricing models and the stylized facts. Kiel Institute for the World Economy, Germany Technical Report.
Lux, T., Kaizoji, T., 2007. Forecasting volatility and volume in the tokyo stock market: Long memory, fractality and regime switching. J. Econ. Dyn. Control 31 (6), 1808–1843.
Lux, T., Segnon, M., 2018. The oxford handbook of computational economics and finance. In: Chapter Multifractal Models in Finance: Their Origin, Properties, and Applications. Oxford University Press.
Lux, T., Zwinkels, R.C., Hommes, C., LeBaron, B., 2018. Chapter 8: empirical validation of agent-based models. In: Handbook of Computational Economics, Vol. 4. Elsevier, pp. 437–488.
Mandelbrot, B., Fisher, A., Calvet, L., 1997. A multifractal model of asset returns. Cowles Found. Discuss. Pap. 1164, 1–33.
Morales, R., Matteo, T.D., Gramatica, R., Aste, T., 2012. Dynamical generalized hurst exponent as a tool to monitor unstable periods in financial time series. Phys. A Stat. Mech. Appl. 391, 3180–3189.
Nakao, H., 2000. Multi-scaling properties of truncated Lévy flights. Phys. Lett. A 266 (4-6), 282–289.
Pamuła, G., Grech, D., 2014. Influence of the maximal fluctuation moment order $q$ on multifractal records normalized by finite-size effects. Europhys. Lett. 105 (5), 50004.
Peng, C., Buldyrev, S., Goldberger, A., Havlin, S., Simons, M., Stanley, H., 1993. Finite-size effects on long-range correlations: Implications for analyzing DNA sequences. Phys. Rev. E 47 (5), 3730–3733.
Platt, D., 2019. A comparison of economic agent-based model calibration methods. Mathematical Institute & INET, University of Oxford Technical Report.
Polach, J., Kukacka, J., 2019. Prospect theory in the heterogeneous agent model. J. Econ. Interact. Coord. 14 (1), 147–174.
Recchioni, M., Tedeschi, G., Gallegati, M., 2015. A calibration procedure for analyzing stock price dynamics in an agent-based framework. J. Econ. Dyn. Control 60, 1–25.
Samorodnitsky, G., 2006. Long range dependence. Found. Trends Stoch. Syst. 1 (3), 163–257.
Schelling, T.C., 1971. Dynamic models of segregation. J. Math. Sociol. 1 (2), 143–186.
Schmitt, N., 2019. Heterogeneous expectations and asset price dynamics. In: Macroeconomic Dynamics. Forthcoming
Schmitt, N., Westerhoff, F., 2017. Heterogeneity, spontaneous coordination and extreme events within large-scale and small-scale agent-based financial market models. J. Evol. Econ. 27 (5), 1041–1070.
Shang, Y., 2014. An agent based model for opinion dynamics with random confidence threshold. Commun. Nonlinear Sci. Numer. Simul. 19 (10), 3766–3777.
da Silva, L., Stauffer, D., 2001. Ising-correlated clusters in the cont-bouchaud stock market model. Phys. A Stat. Mech. Appl. 294 (1), 235–238.
Stauffer, D., 2008. Social applications of two-dimensional ising models. Am. J. Phys. 76 (4), 470–473.
Theiler, J., Eubank, S., Longtin, A., Galdrikian, B., Farmer, J.D., 1992. Testing for nonlinearity in time series: the method of surrogate data. Phys. D 58, 77–94.
Thom, R., 1975. Structural Stability and Morpohogenesis. Benjamin, New York..
Vandewalle, N., Ausloos, M., 1998. Crossing of two mobile averages: a method for measuring the roughness exponent. Phys. Rev. E. 58, 6832–6834.
Veneziano, D., Langousis, A., Furcolo, P., 2006. Multifractality and rainfall extremes: a review. Water Resour. Res. 42 (6), W06D15.
Windrum, P., Fagiolo, G., Moneta, A., 2007. Empirical validation of agent-based models: alternatives and prospects. J. Artif. Soc. Soc. Simul. 10 (2), 8.
Zeeman, E.C., 1974. On the unstable behaviour of stock exchanges. J. Math. Econ. 1, 39–49.
Zhang, L., Mykland, P., Aït-Sahalia, Y., 2005. A tale of two time scales: determining integrated volatility with noisy high frequency data. J. Am. Stat. Assoc. 100 (472), 1394–1411.
Zhou, W.X., 2009. The components of empirical multifractality in financial returns. Europhys. Lett. 88 (2), 28004.
Zuo, R., Wang, J., 2016. Fractal/multifractal modeling of geochemical data: a review. J. Geochem. Explor. 164, 33–41.